We have a 7T ...
Now what?

Souheil Inati
FMRI Course
August 30, 2011

Interrupt early and often.

7T Upside and Downside

- Upside
  - More SNR
  - More CNR (for some contrasts)
- Downside
  - More B_0 inhomogeneity
  - More B_1 inhomogeneity
  - More RF absorption (SAR)
  - Worse CNR (for some contrasts)

FMRIF

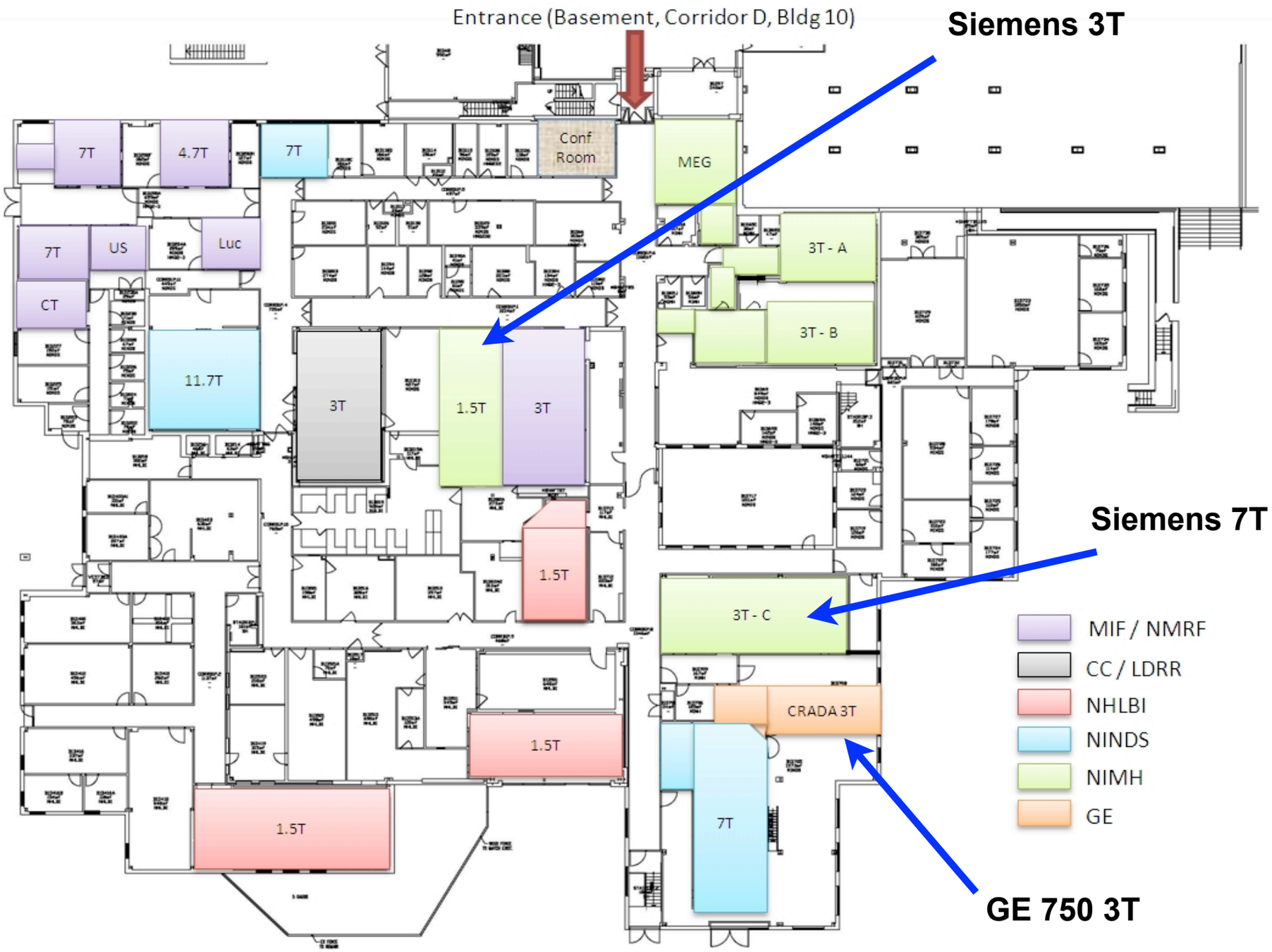
Entrance (Basement, Corridor D, Bldg 10)
Siemens 3T
Siemens 7T
GE 750 3T
7T
4.7T
7T
Conf. Room
MEG
7T
US
Luc
CT
11.7T
3T
1.5T
3T
3T - A
3T - B
1.5T
3T - C
CRADA 3T
1.5T
7T
1.5T
MIF / NMRF
CC / LDRR
NHLBI
NINDS
NIMH
GE

Installation and Tune-Up

Magnet Delivery – 08/15/10

Magnex/Agilent 7T/830 Actively shielded

Installation Complete – 11/08/10

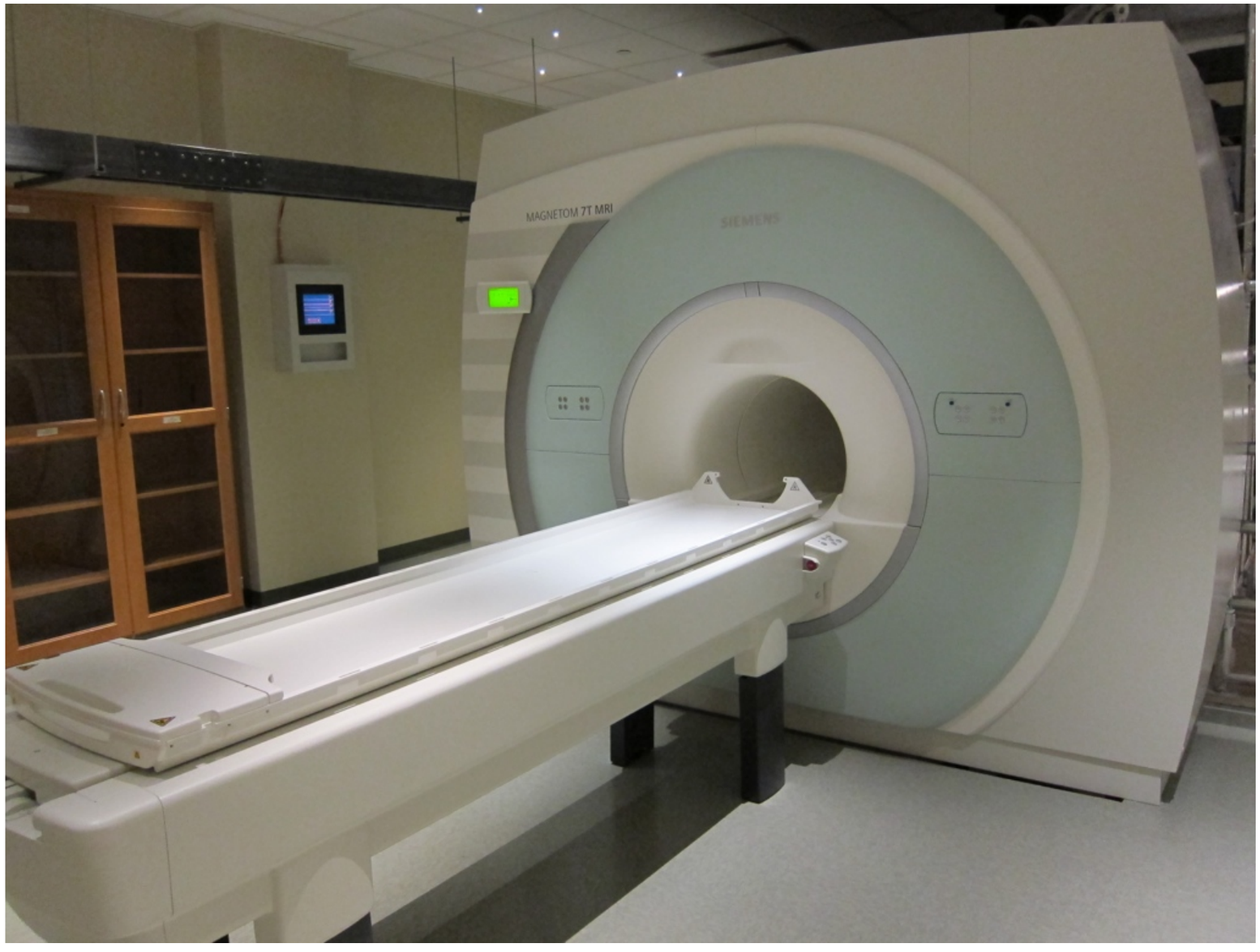

Followed by lots of Siemens testing ...
Human investigational study release 12/13/10

Fruits and Vegetables - 11/17/10

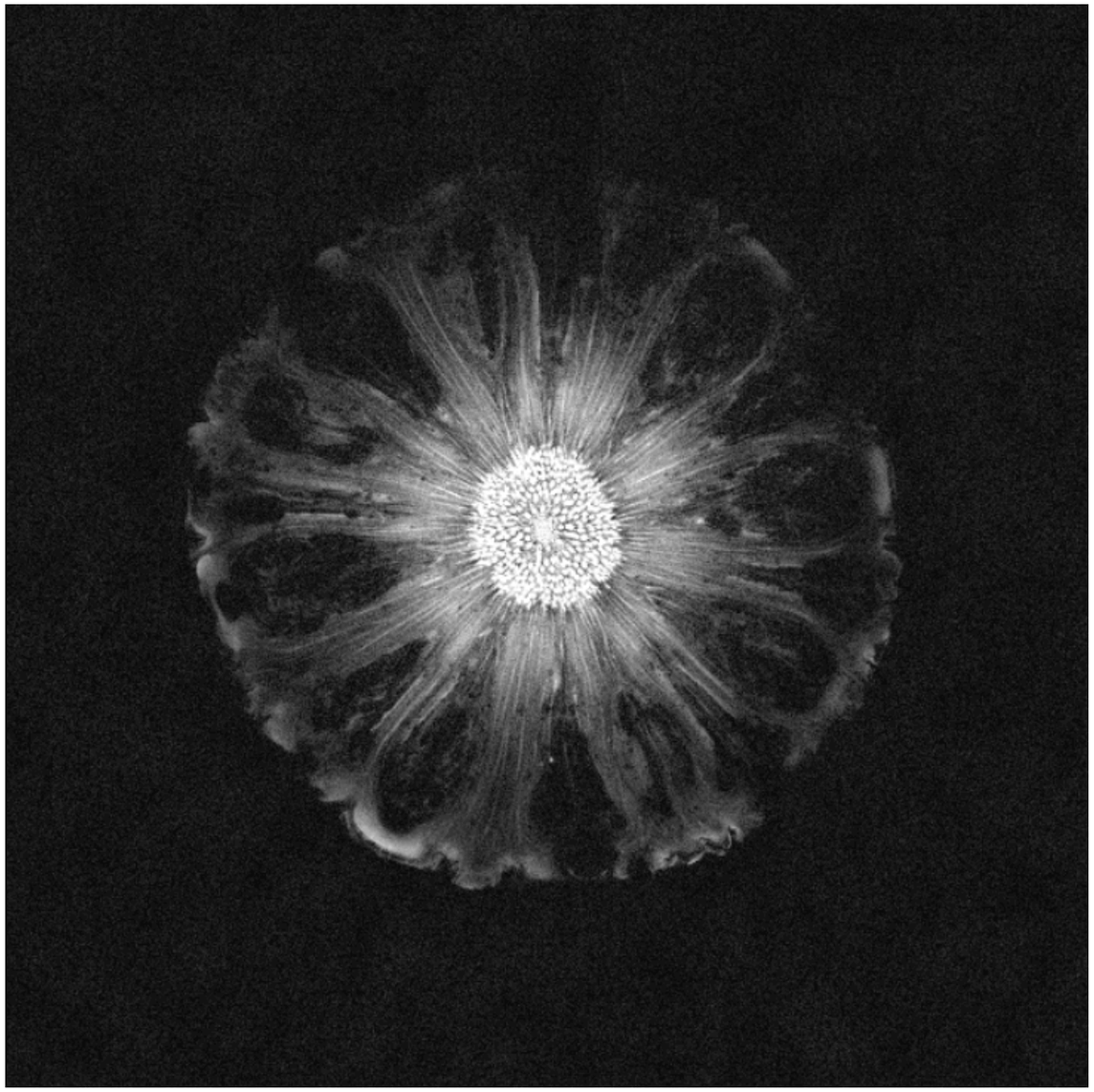

Pineapple

Onion

First Functional Scan – 12/13/10

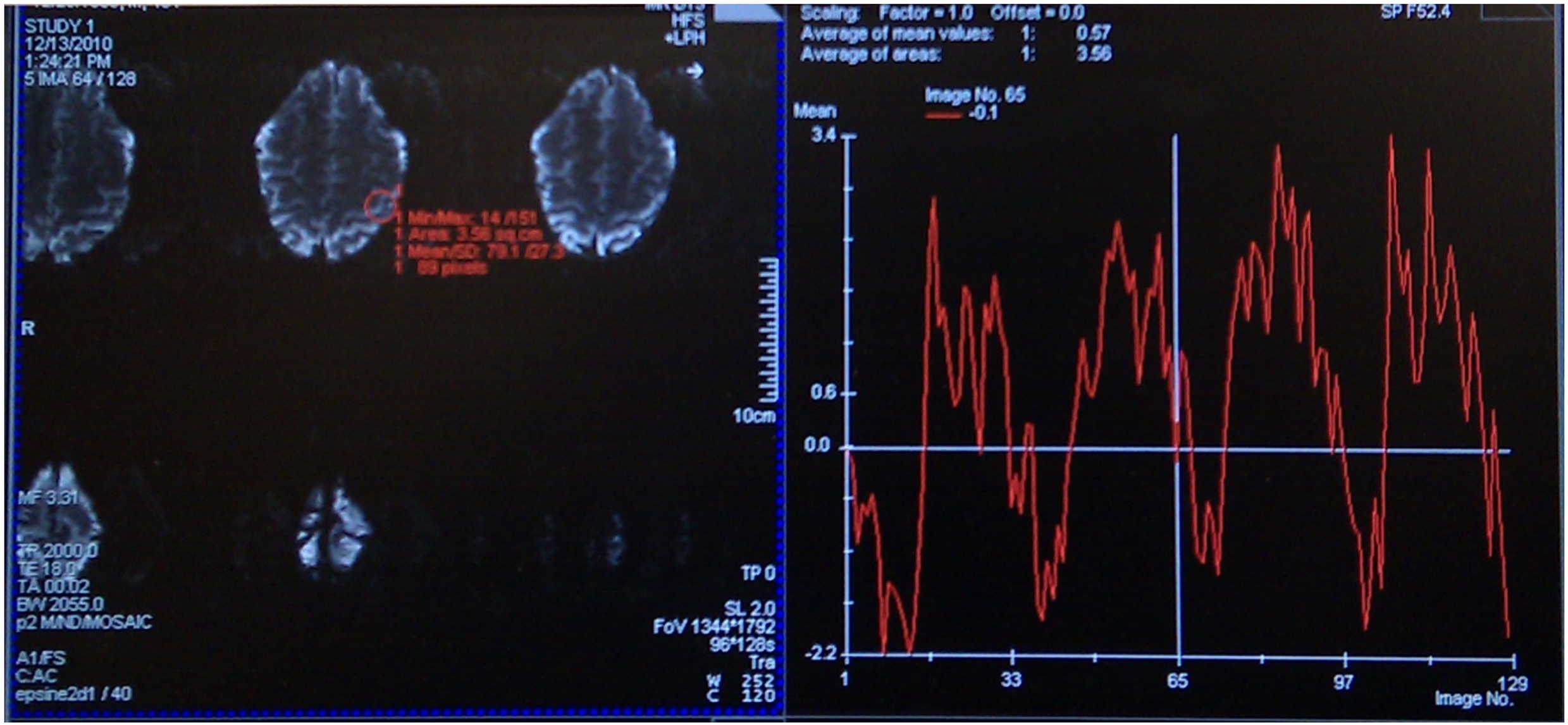

Subject SM - finger tapping

Hardware

System Specs

- Magnex/Agilent 7T/830 Actively shielded
- Siemens console (VB15 → VB17 next week)
- Siemens gradient SC72
  - Gmax = 42 mT/m, Gmax* = 70 mT/m
  - Slew Rate = 200 mT/m/ms
  - Partial 3rd Order Shim
- Siemens electronics
  - Single channel Tx (1H and broadband X)
  - 32 channel Rx

RF Coils

- Nova 32
- QED $^{1}H/^{31}P$
- Siemens Birdcage
- Home built coils
  - Spine array
  - Others

RF Coils: Nova 32

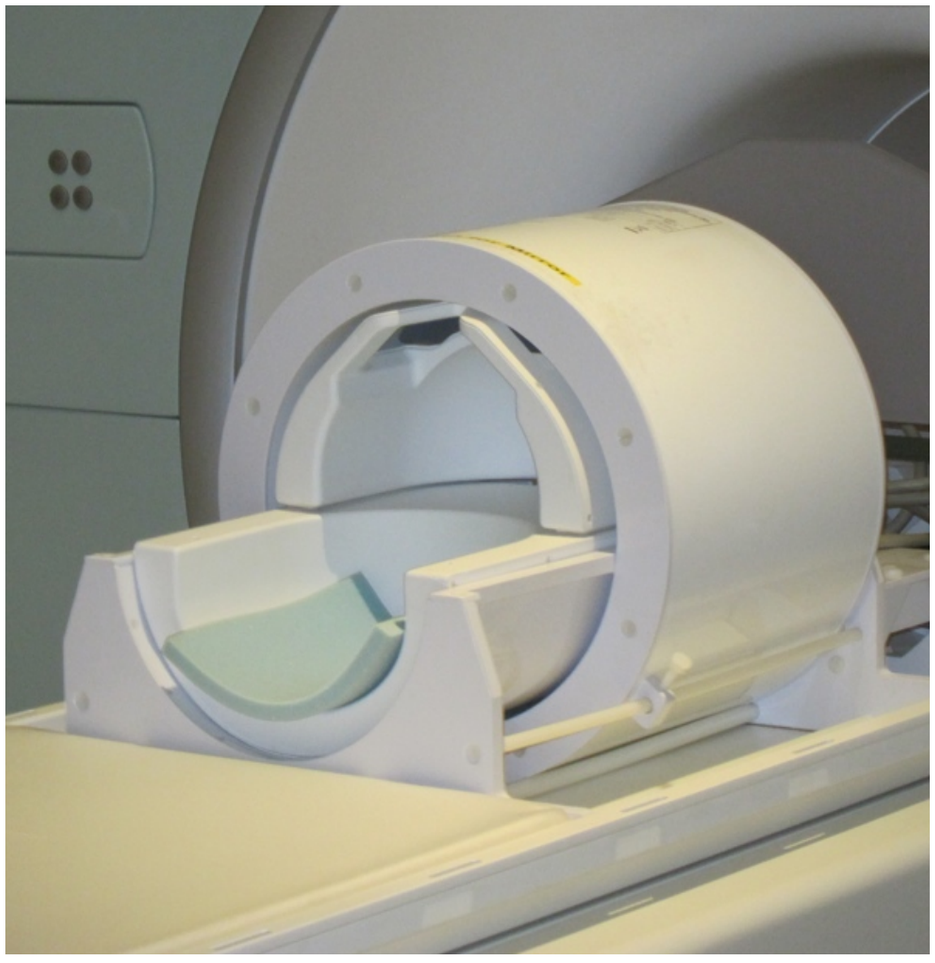

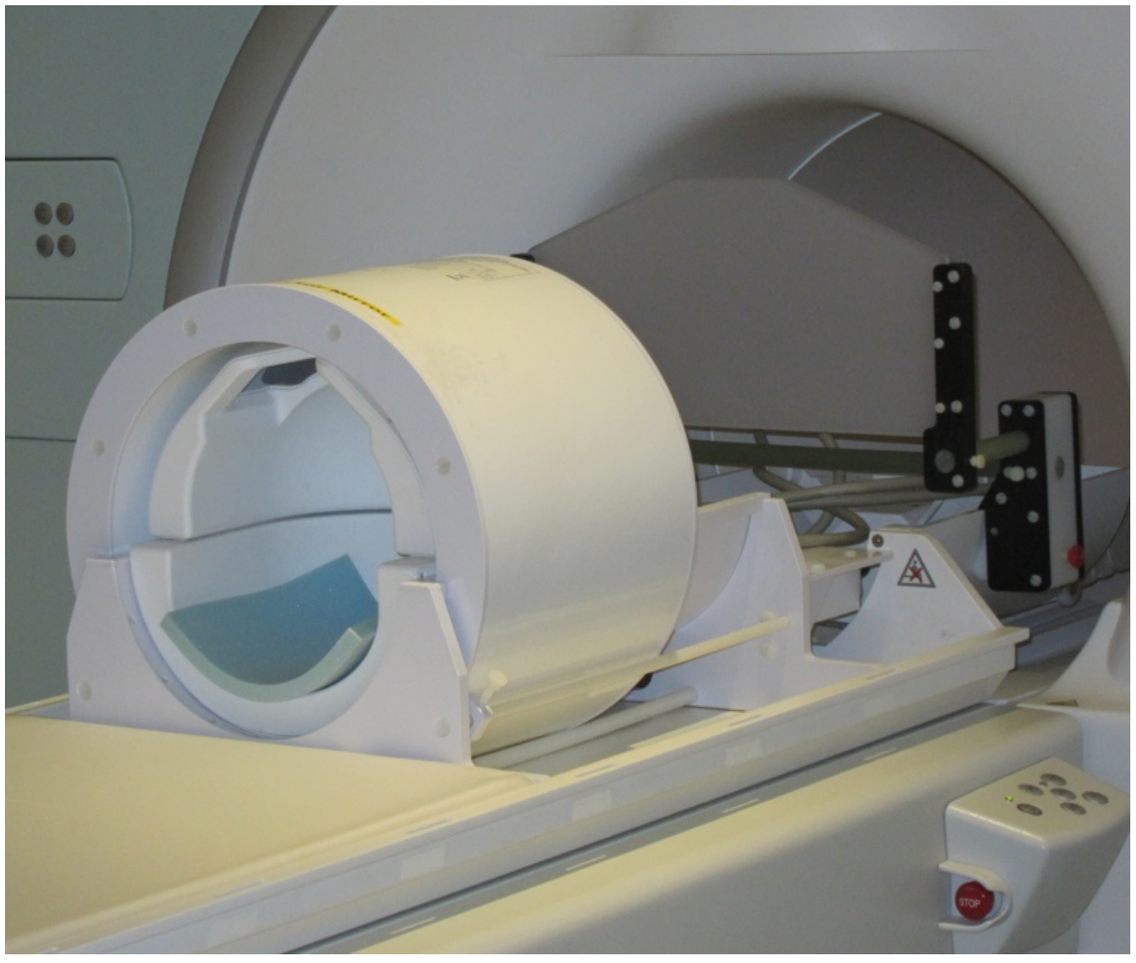

Nova Medical: volume transmit, 32 channel receive array

RF Coils: QED Dual Tuned $^{1}H/^{31}P$

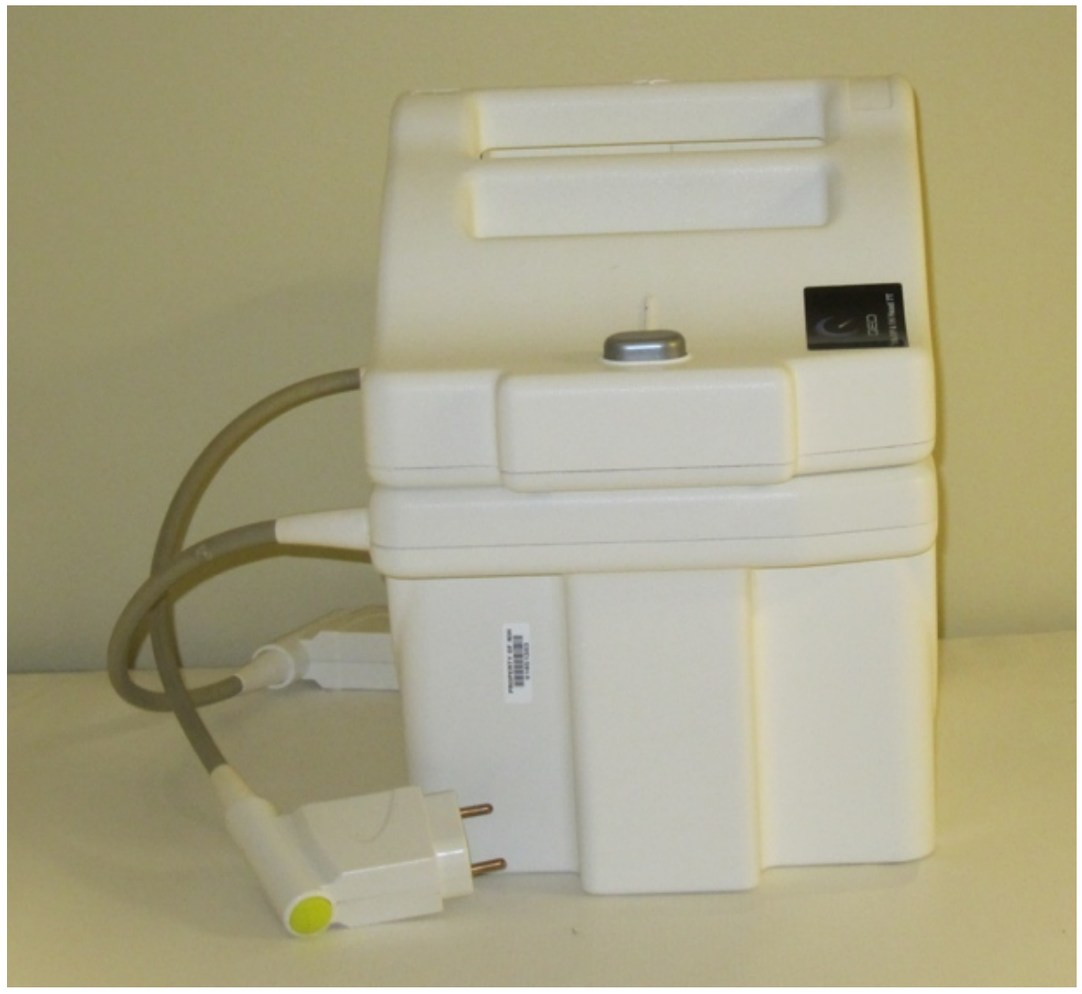

NINDS

RF Coils: Siemens Birdcage

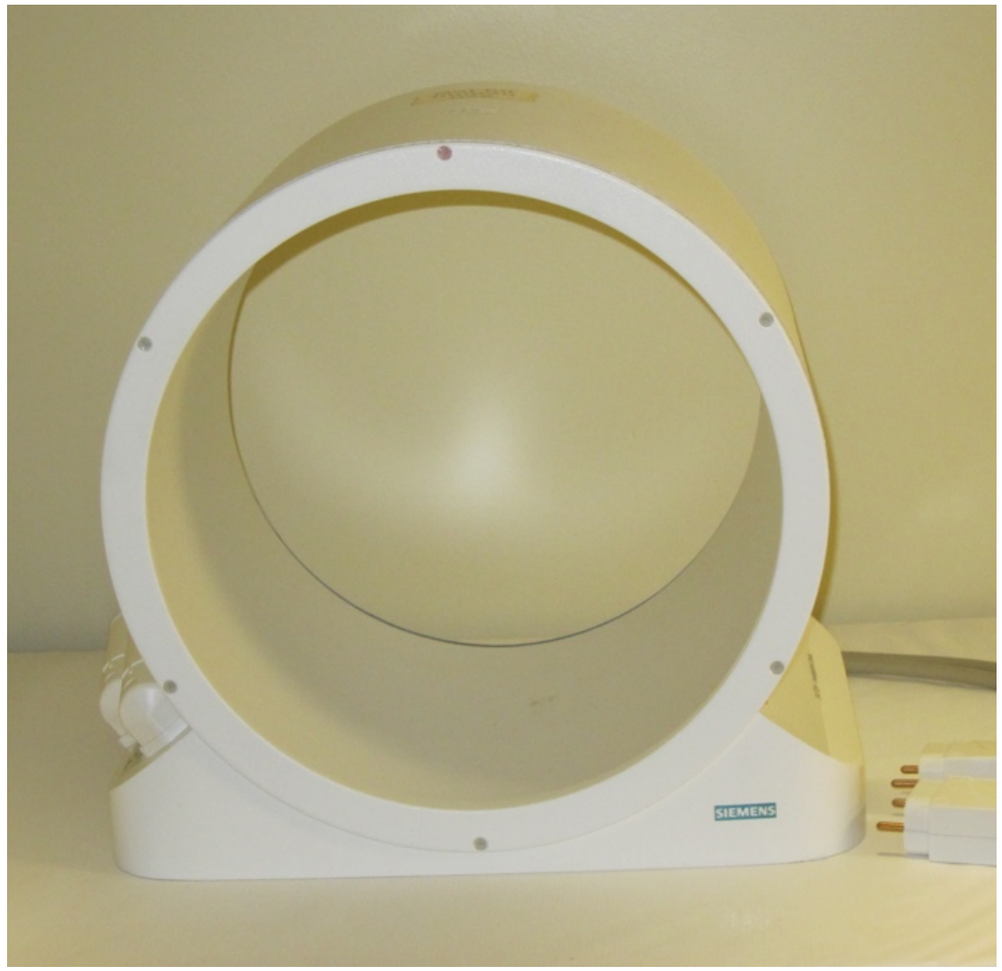

Quadrature Birdcage

not yet approved for human use

7T Upside and Downside

- Upside
  - More SNR
  - More CNR (for some contrasts)
- Downside
  - More B_0 inhomogeneity
  - More B_1 inhomogeneity
  - More RF absorption (SAR)
  - Worse CNR (for some contrasts)

More SNR is good

More SNR is good

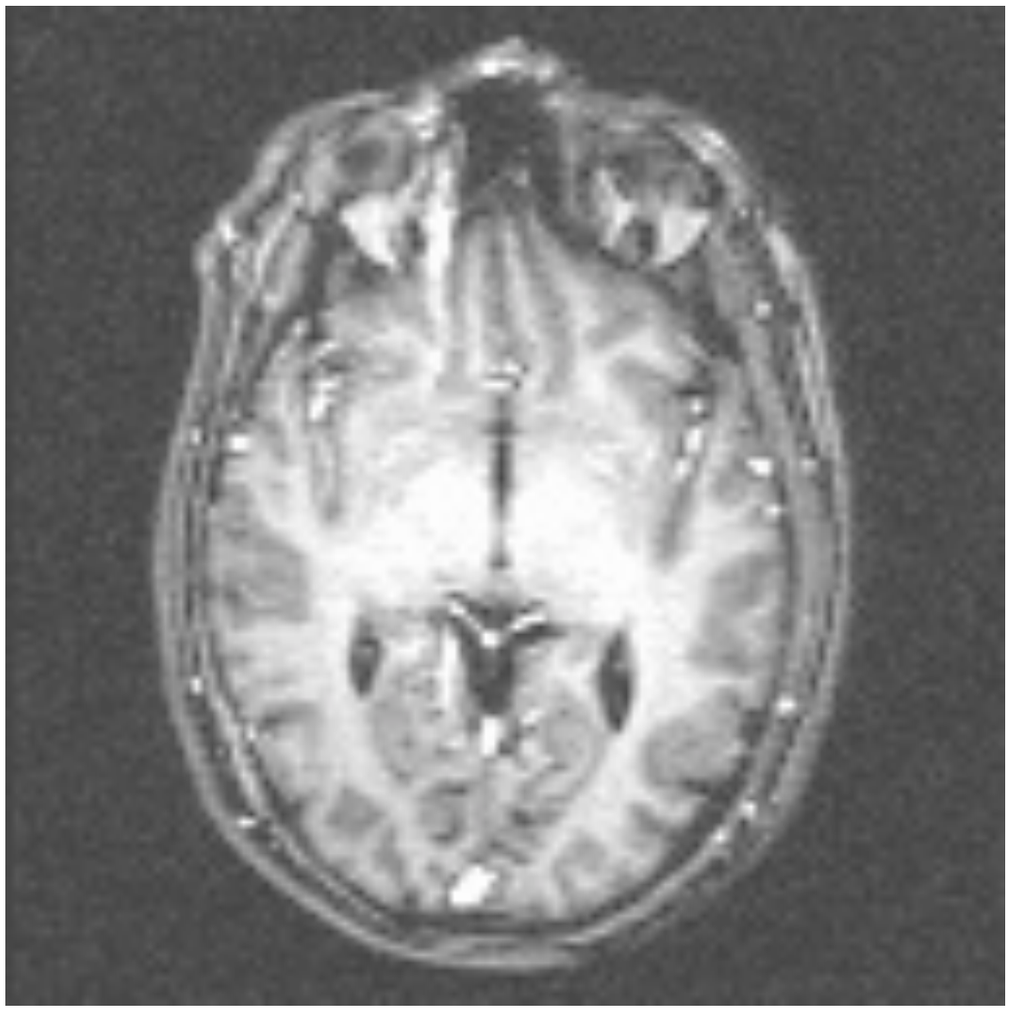

1 mm, 10 min
3T, Volume Coil

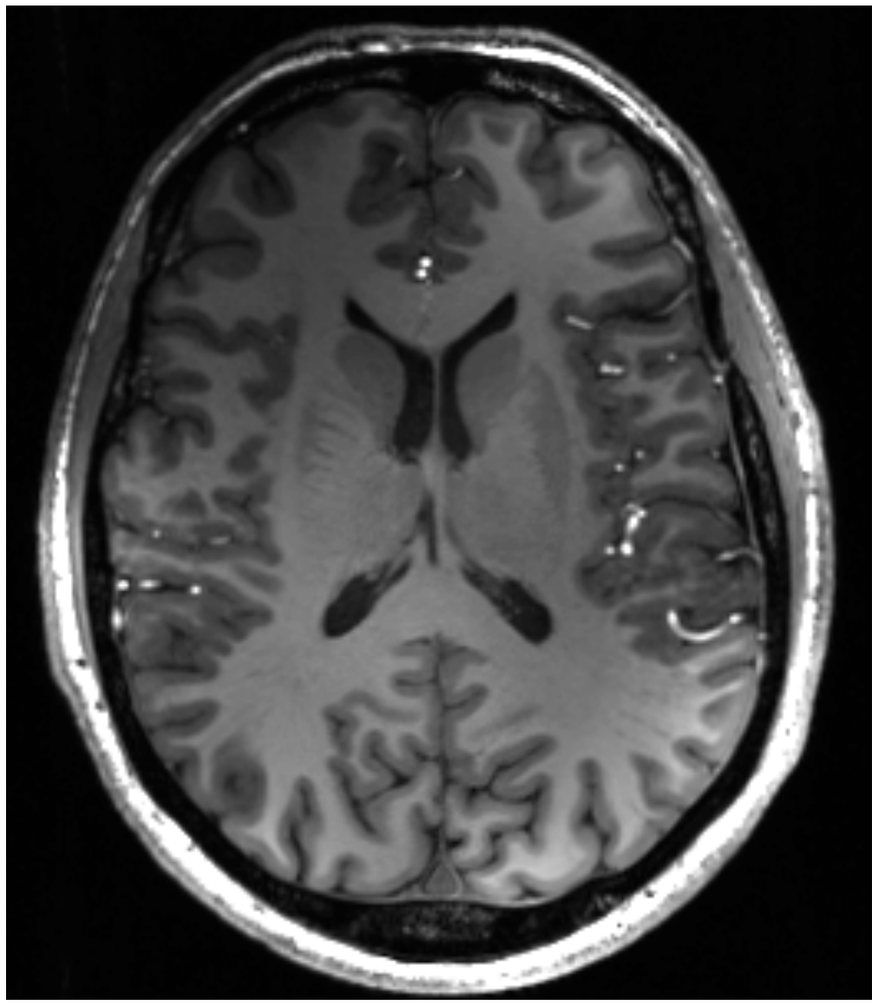

0.7 mm, 10 min
7T, Rcv Array

Anatomy

0.7 mm iso

MPRAGE

Proton Density

Normalized

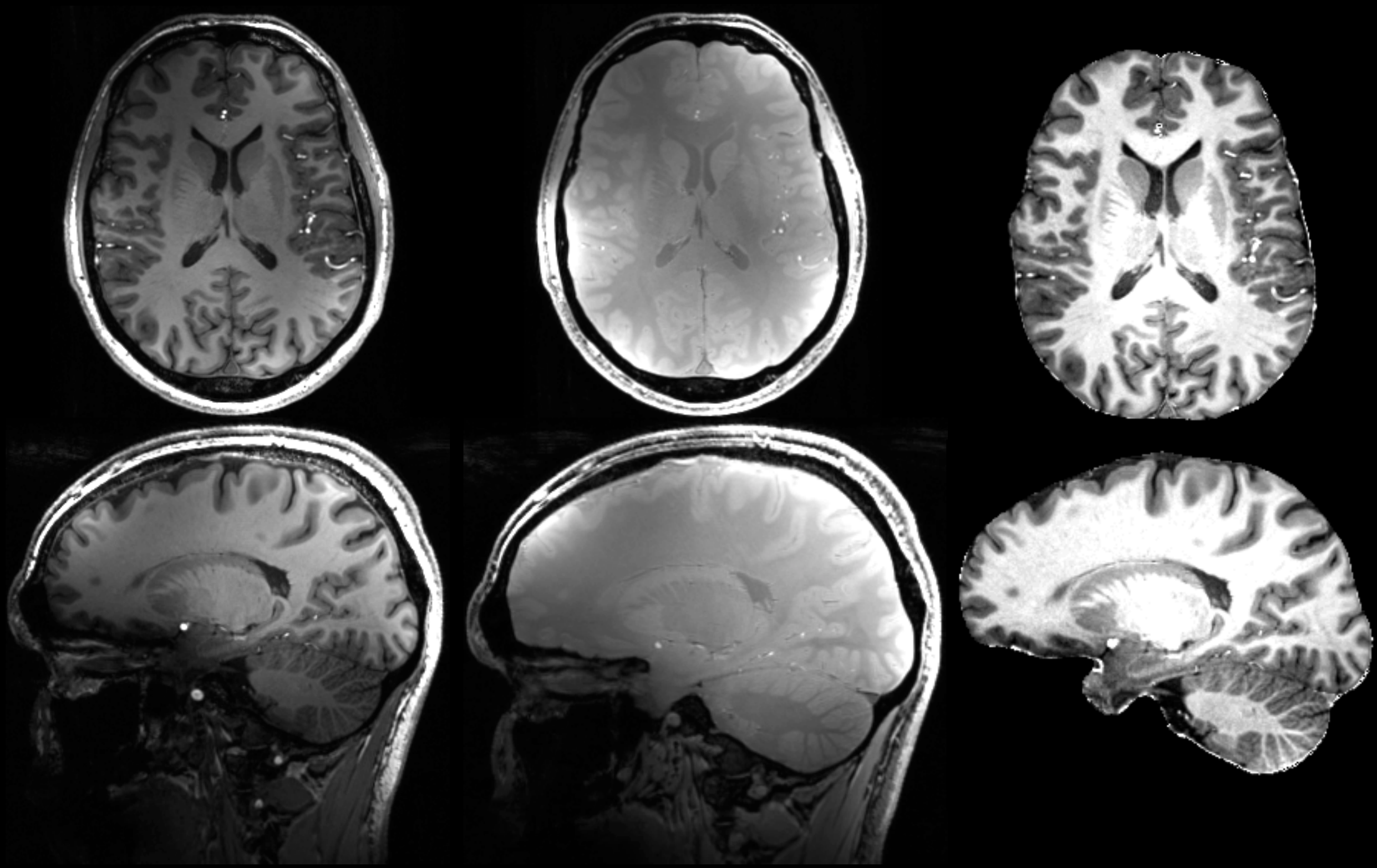

Angiography

JOURNAL OF MAGNETIC RESONANCE IMAGING 32:544–550 (2010)

Original Research

Non-Invasive Visualization of Basilar Artery Perforators With 7T MR Angiography

Chang-Ki Kang, PhD,[1] Chan-A Park, MS,[1] Kyoung-Nam Kim, MS,[1] Suk-Min Hong, MS,[1] Cheol-Wan Park, MD, PhD,[1] Young-Bo Kim, MD, PhD,[1] and Zang-Hee Cho, PhD[1,2*]

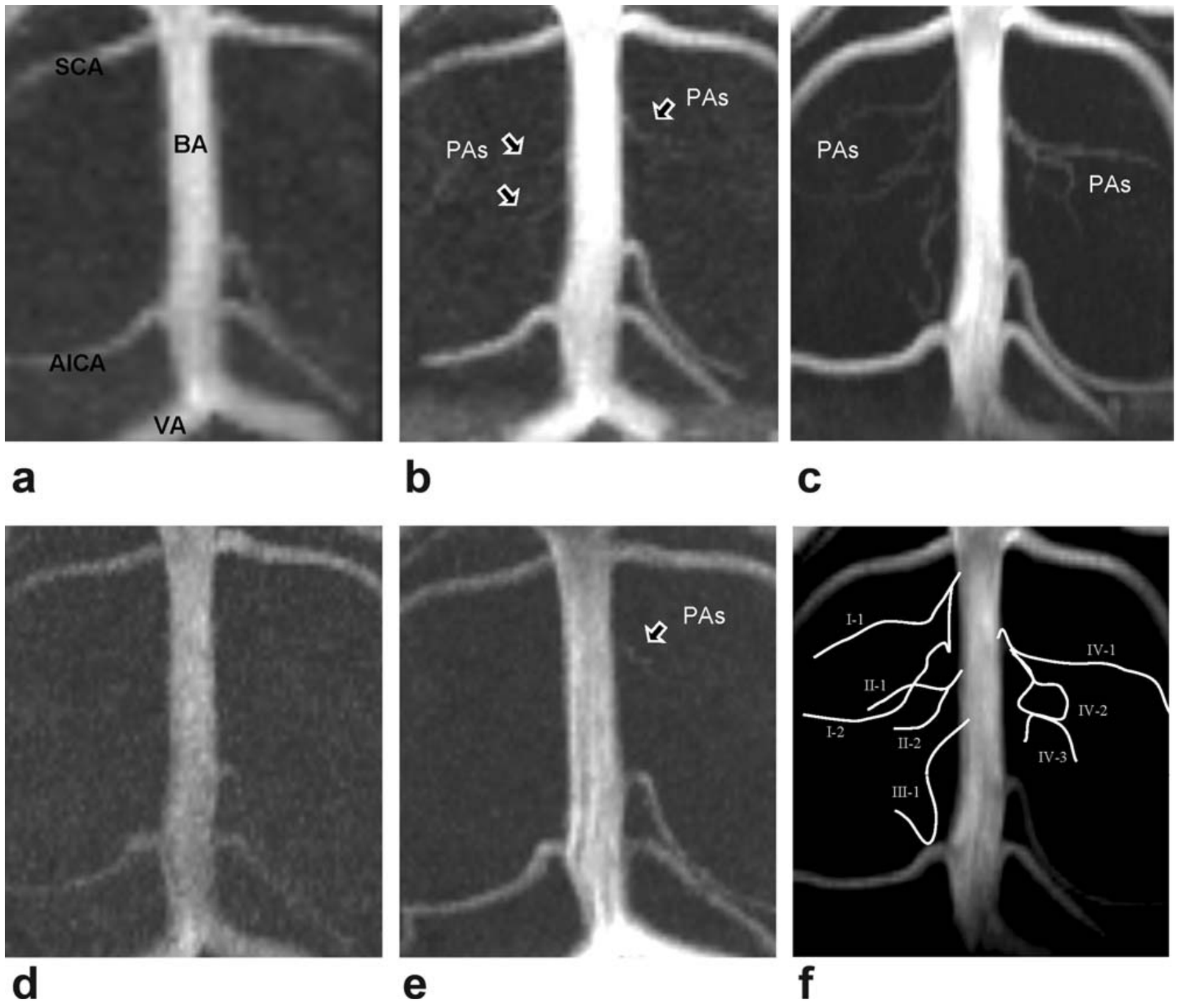

Figure 5. Comparison of PAs with 7T MRI and conventional lower field MRIs. PA images obtained with optimized MR parameters with 1.5T and 3T MRIs are shown in (**a**, **d**) and (**b**, **e**), respectively. Faint branches of the PAs visualized by 3T MRI are indicated by the arrows. A PA image obtained by 7T MRI and its corresponding line drawing are shown in (**c**) and (**f**), respectively. (a), (b), and (c) were obtained with the same temporal resolution as shown in Table 1, and (d) and (e) with the same spatial resolution as that of 7T MRA, but longer acquisition time as shown in Table 1.

Angiography

1.5T

3T

7T

Comparison of Magnetic Resonance Angiography Scans on 1.5, 3, and 7 Tesla Units: A Quantitative Study of 3-Dimensional Cerebrovasculature

Wieslaw L. Nowinski, DSc, PhD, Fiftarina Puspitasaari, BEng, Ihar Volkau, PhD, Yevgen Marchenko, MSc, Michael V. Knopp, MD, PhD

From the Biomedical Imaging Lab, Agency for Science Technology and Research, Singapore (WLN, FP, IV, YM); Department of Radiology, Wright Center of Innovation, The Ohio State University, OH (MVK).

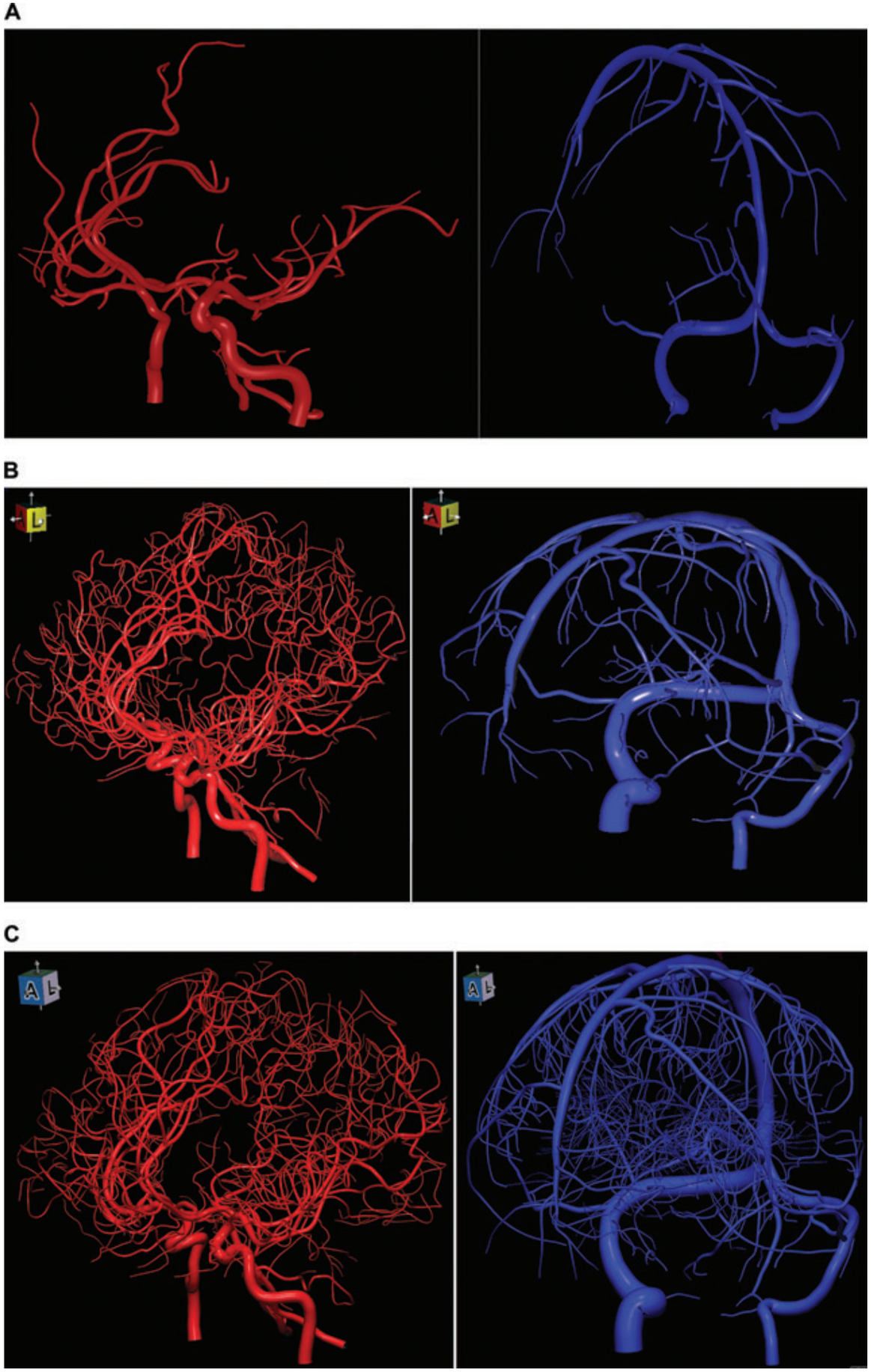

Trabecular bone

Magn Reson Mater Phy (2011) 24:191–199
DOI 10.1007/s10334-011-0252-0

RESEARCH ARTICLE

Quantitative assessment of trabecular bone micro-architecture of the wrist via 7 Tesla MRI: preliminary results

Gregory Chang · Ligong Wang · Guoyuan Liang · James S. Babb · Graham C. Wiggins · Punam K. Saha · Ravinder R. Regatte

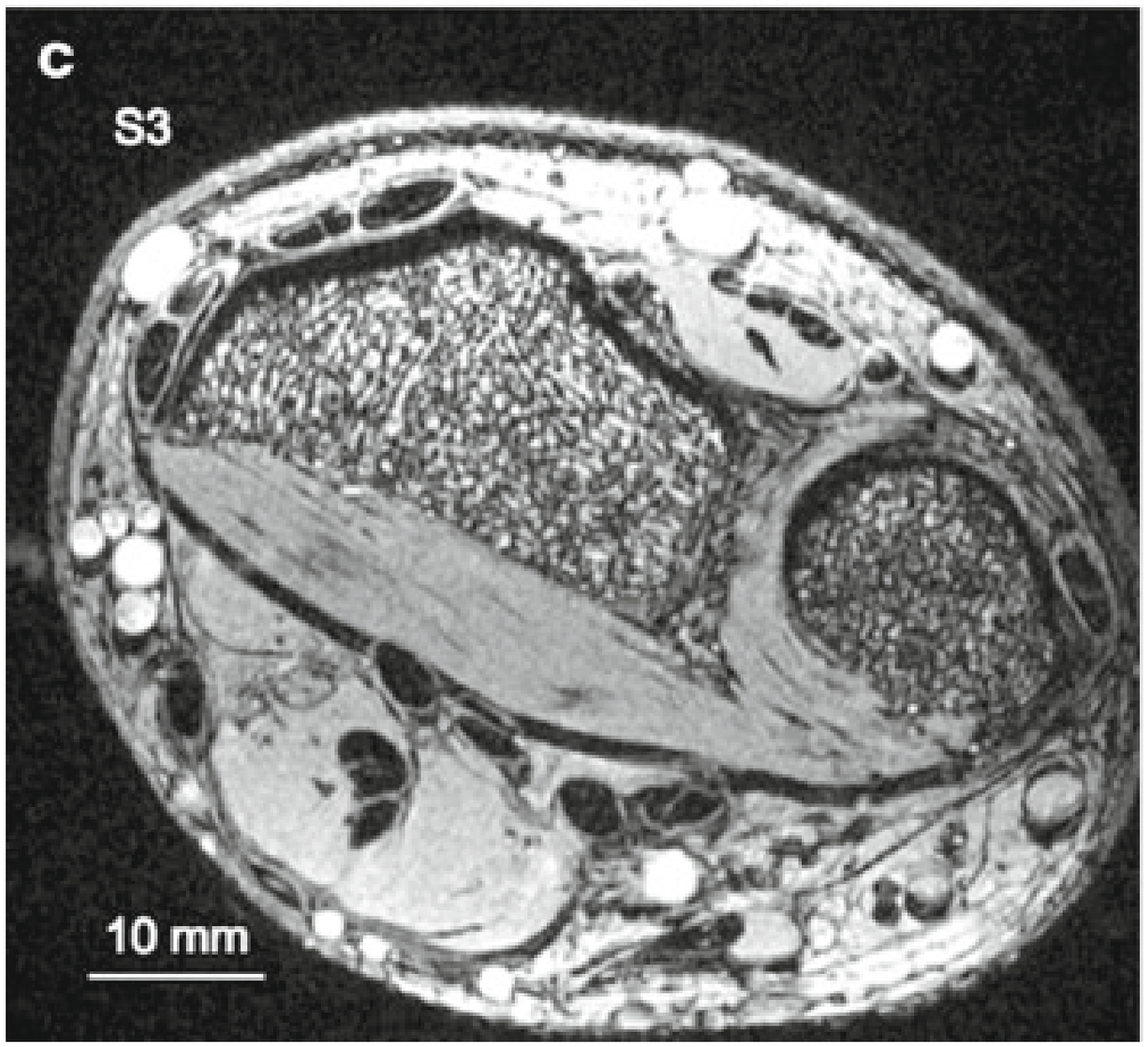

Imaging other nuclei

Sodium in the knee

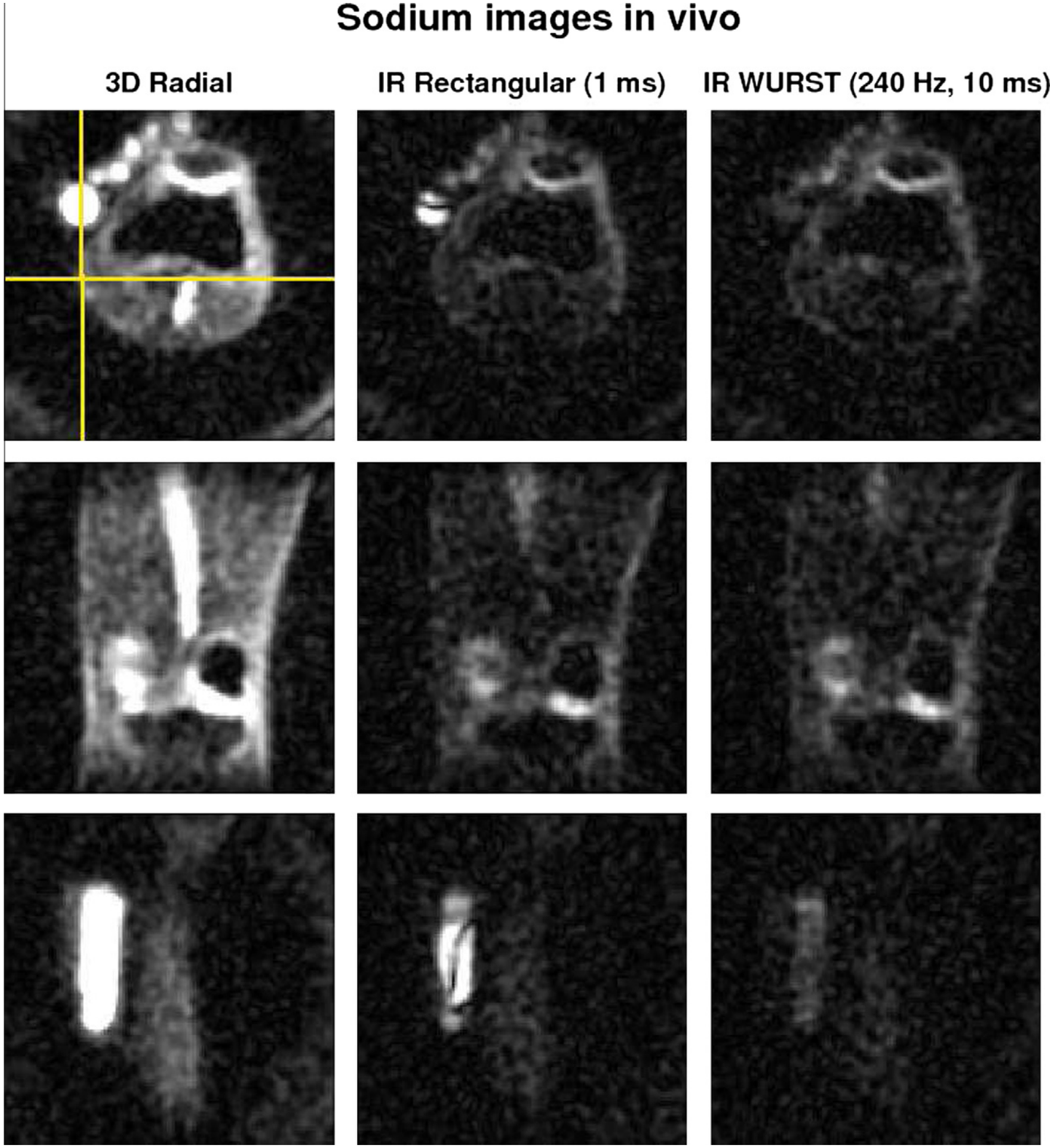

Journal of Magnetic Resonance 207 (2010) 42–52

Contents lists available at ScienceDirect

Journal of Magnetic Resonance

journal homepage: www.elsevier.com/locate/jmr

Sodium inversion recovery MRI of the knee joint in vivo at 7T

Guillaume Madelin [a,b], Jae-Seung Lee [a,b], Souheil Inati [c], Alexej Jerschow [b,*], Ravinder R. Regatte [a,**]

[a] *Center for Biomedical Imaging, New York University Medical Center, New York, NY, USA*
[b] *Chemistry Department, New York University, New York, NY 10012, USA*
[c] *NIH, Bethesda, MD, USA*

Spectroscopy

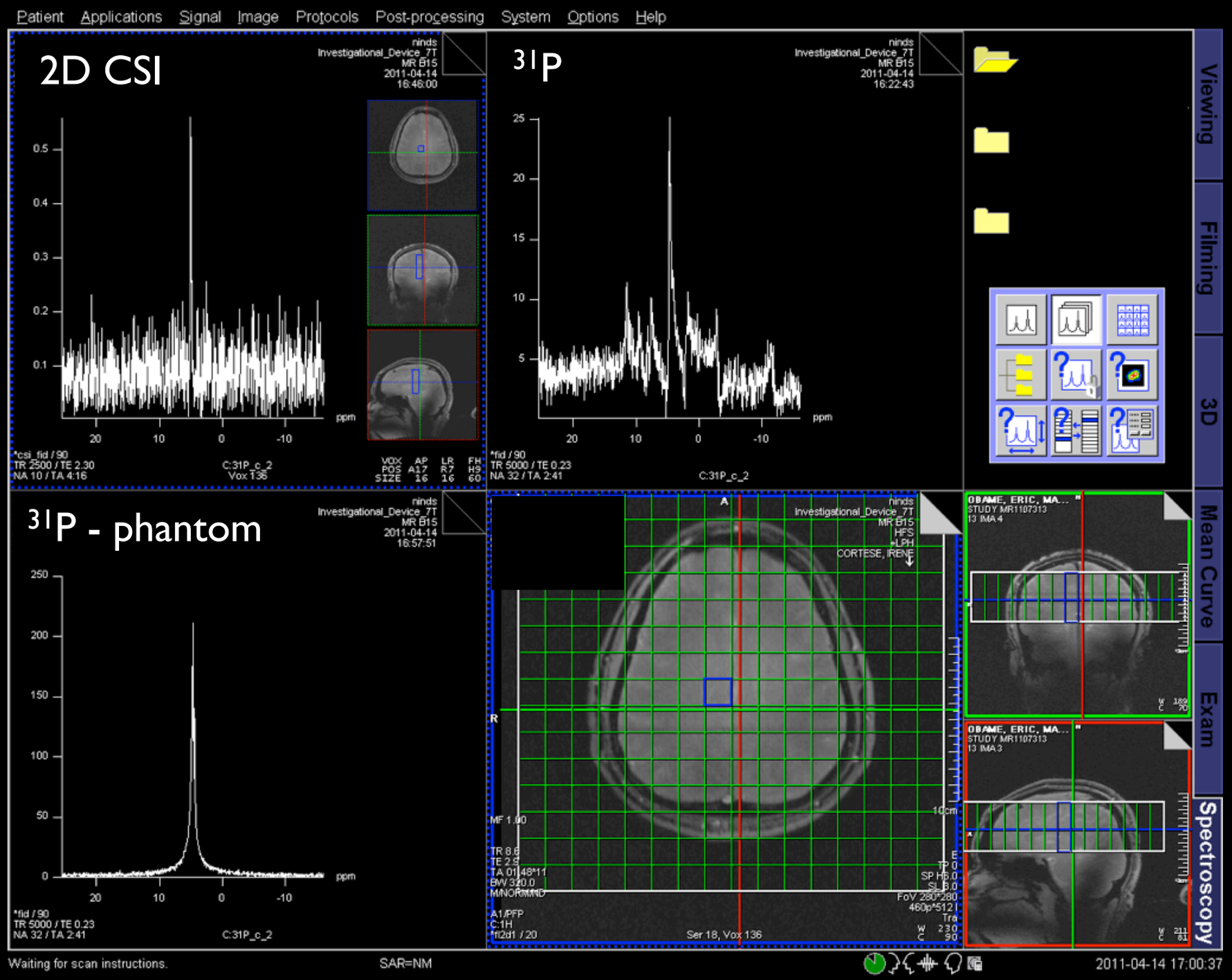

Pascal Sati, Steve Li

SNR for resolution

High Resolution Anatomy

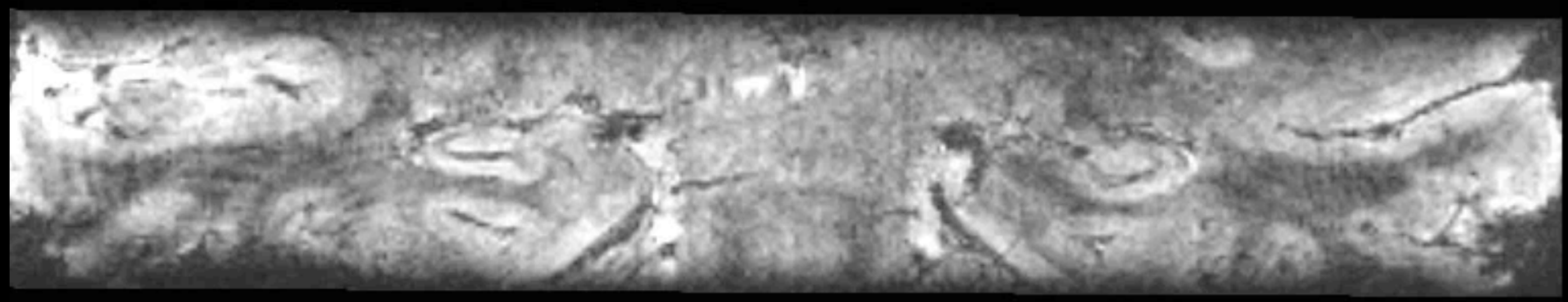

GRE imaging of the hippocampus
0.4mm iso, 512x448x60
TE=30ms, TR=50ms, FA=10°
TA=8min

AN

High resolution diffusion

Magnetic Resonance in Medicine 64:9–14 (2010)

Diffusion Imaging in Humans at 7T Using Readout-Segmented EPI and GRAPPA

Robin M. Heidemann,[1]* David A. Porter,[2] Alfred Anwander,[1] Thorsten Feiweier,[2] Keith Heberlein,[2] Thomas R. Knösche,[1] and Robert Turner[1]

FIG. 2. High-resolution multi-shot images, acquired using readout-segmented EPI with a nominal pixel size of 0.7 mm × 0.7 mm × 3.0 mm and a *b*-value of 1000 s/mm^2.

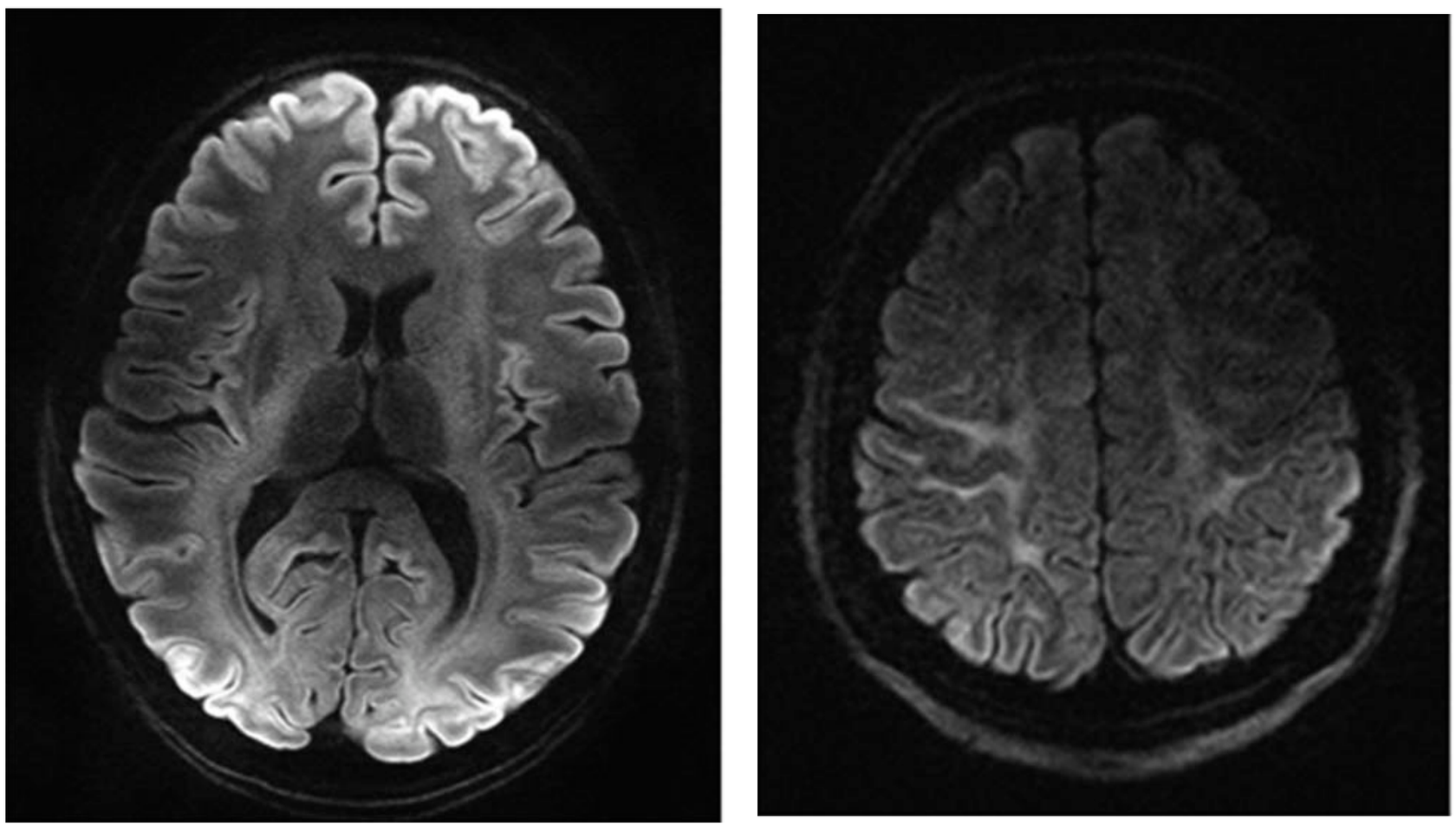

High resolution diffusion

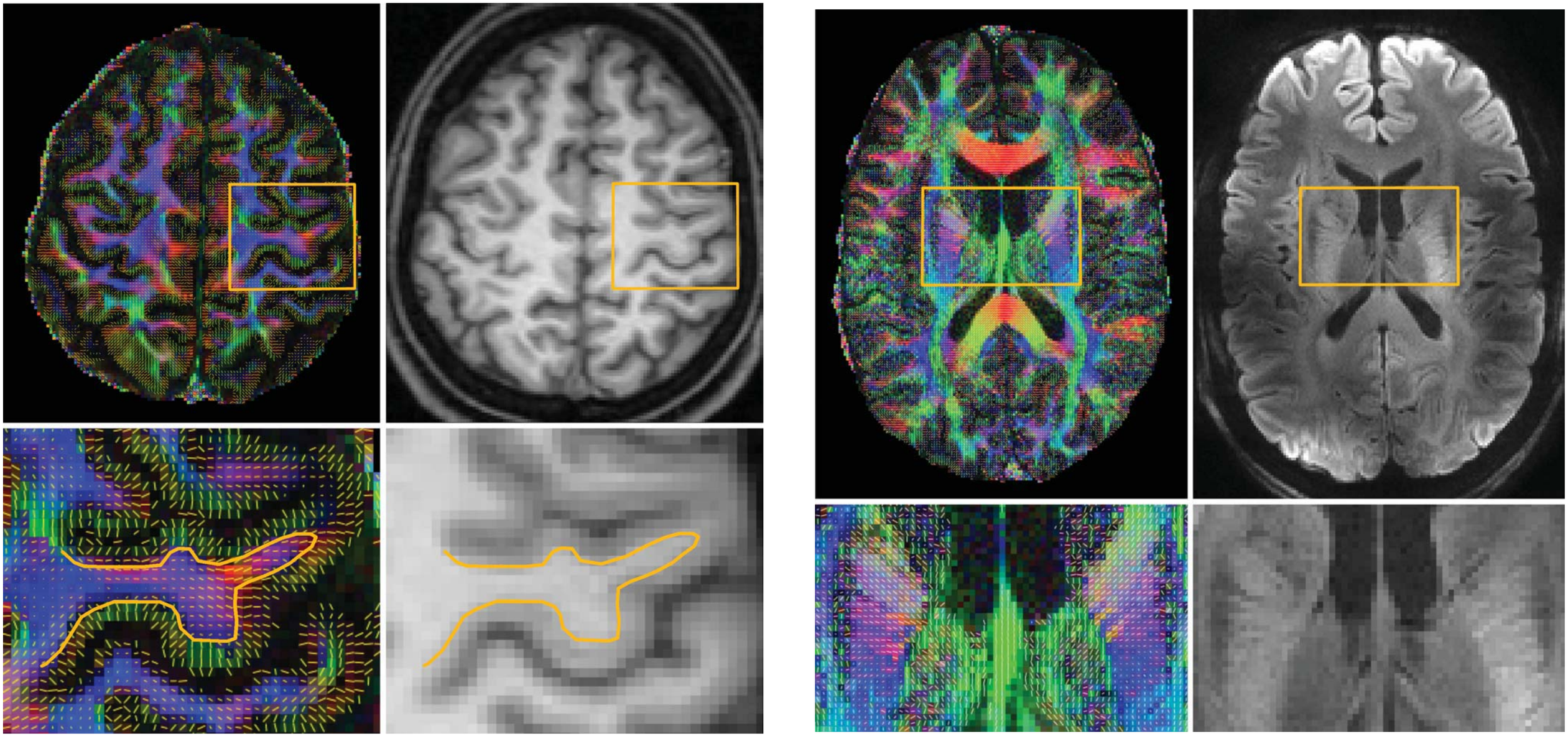

High resolution FMRI

1mm resolution

J Neurophysiol 103: 2544–2556, 2010.
First published February 17, 2010; doi:10.1152/jn.01017.2009.

Mapping Human Somatosensory Cortex in Individual Subjects With 7T $^{c}_{i}$ Functional MRI

R. M. Sanchez-Panchuelo,[1] S. Francis,[1] R. Bowtell,[1] and D. Schluppeck[2]

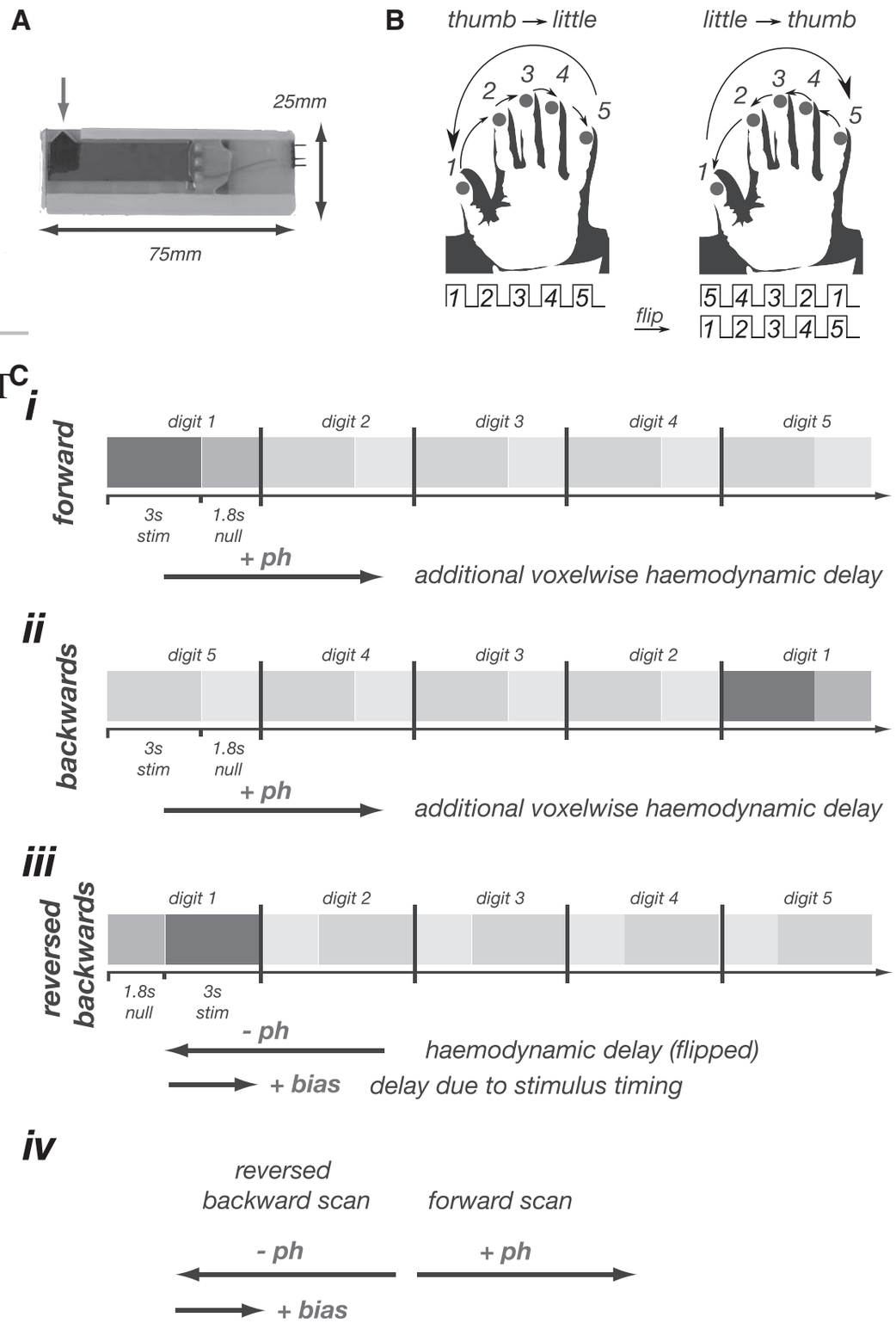

High resolution FMRI

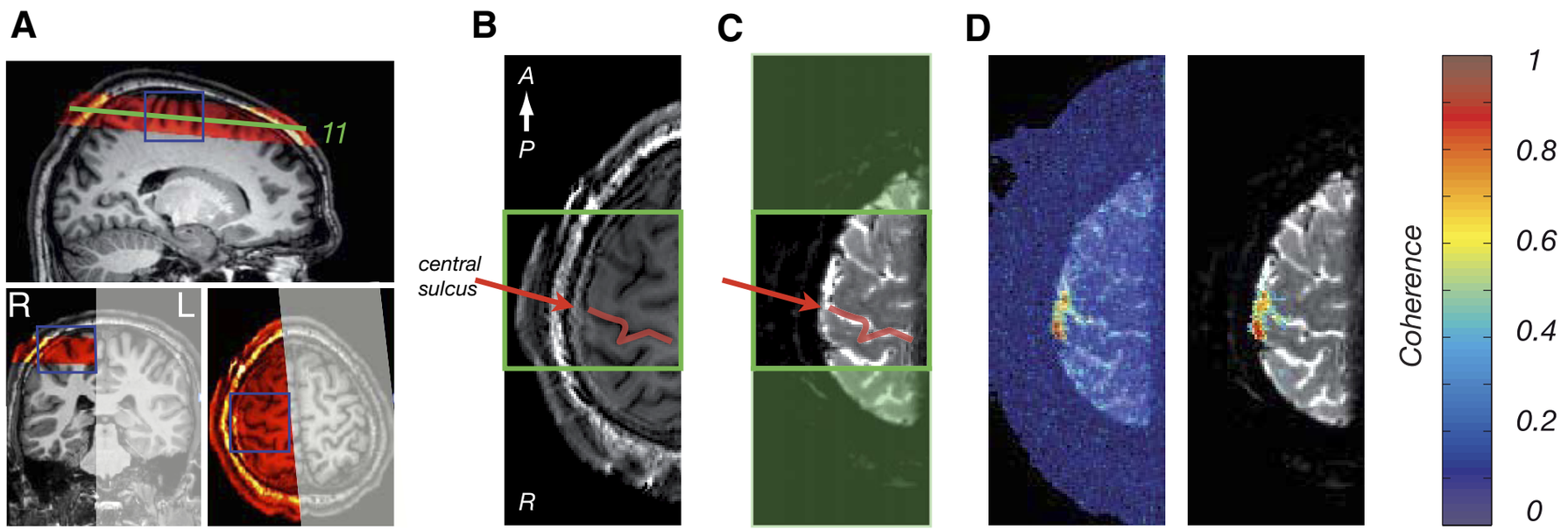

FIG. 3. *A*: location of the imaging stack for zoomed fMRI (red) superimposed on MPRAGE scan for a representative subject. The gray shaded area indicates the location of the outer volume suppression slab and the blue lines show the location of the shim box. *B*: single slice of the MPRAGE image (1 mm isotropic MPRAGE) collected in the same location as the T_2*-weighted EPI data. The red line indicates the location of central sulcus, the green box the cropping used in *E*. *C*: mean T_2* weighted EP image obtained by averaging 100 repeats of 1 functional MRI scan; because fMRI data contain slight residual geometric distortions with respect to the MPRAGE images, statistical images are superimposed on the average EPI data. Red line, as in *B*. *D*: statistical map superimposed on mean EPI image. Transparent colors, coherence with best-fitting sinusoid at frequency of stimulus paradigm. Note values close to 1, indicating high statistical significance. *Left*: no thresholding applied. *Right*: statistical image obtained with threshold-free cluster enhancement, TFCE. *E*: statistical map (from the average of 6 scans) superimposed on mean T_2*-weighted EPI data for all slices in stack. Axial slices are numbered from most superior (1) to most inferior (22). Colors indicate the phase values from traveling wave paradigm. Note that the statistical map is thresholded based on application of TFCE to the coherence map (see *D*). For this subject, the ROI contained 1,998 voxels. The mean coherence value was 0.53 ± 0.13 (minimum-to-maximum range: 0.35–0.94), the mean fMRI response amplitude across all voxels 3.28 ± 3.2% (range: 0.72–21.38), and the mean raw image intensity of the EP image was 22,434 ± 6,957 (range: 4,014–50,071).

High resolution FMRI at NIH

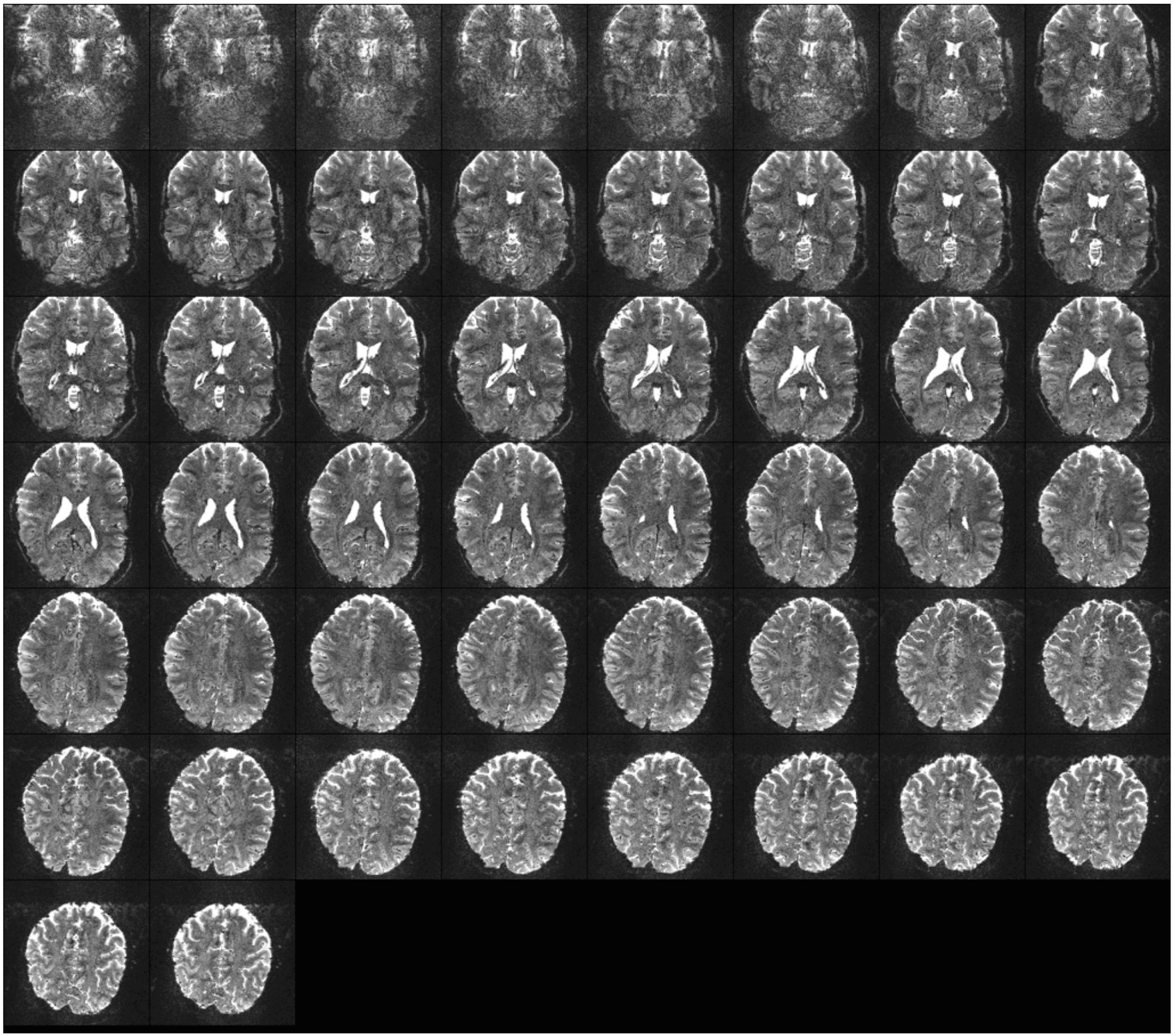

0.75mm iso
50 slices
TR = 4s

SNR for Speed

EPI for anatomy

Fast high resolution whole brain T2* weighted imaging using echo planar imaging at 7 T

Jaco J.M. Zwanenburg [a,b,*], Maarten J. Versluis [d], Peter R. Luijten [a], Natalia Petridou [a,c]

15x speedup!

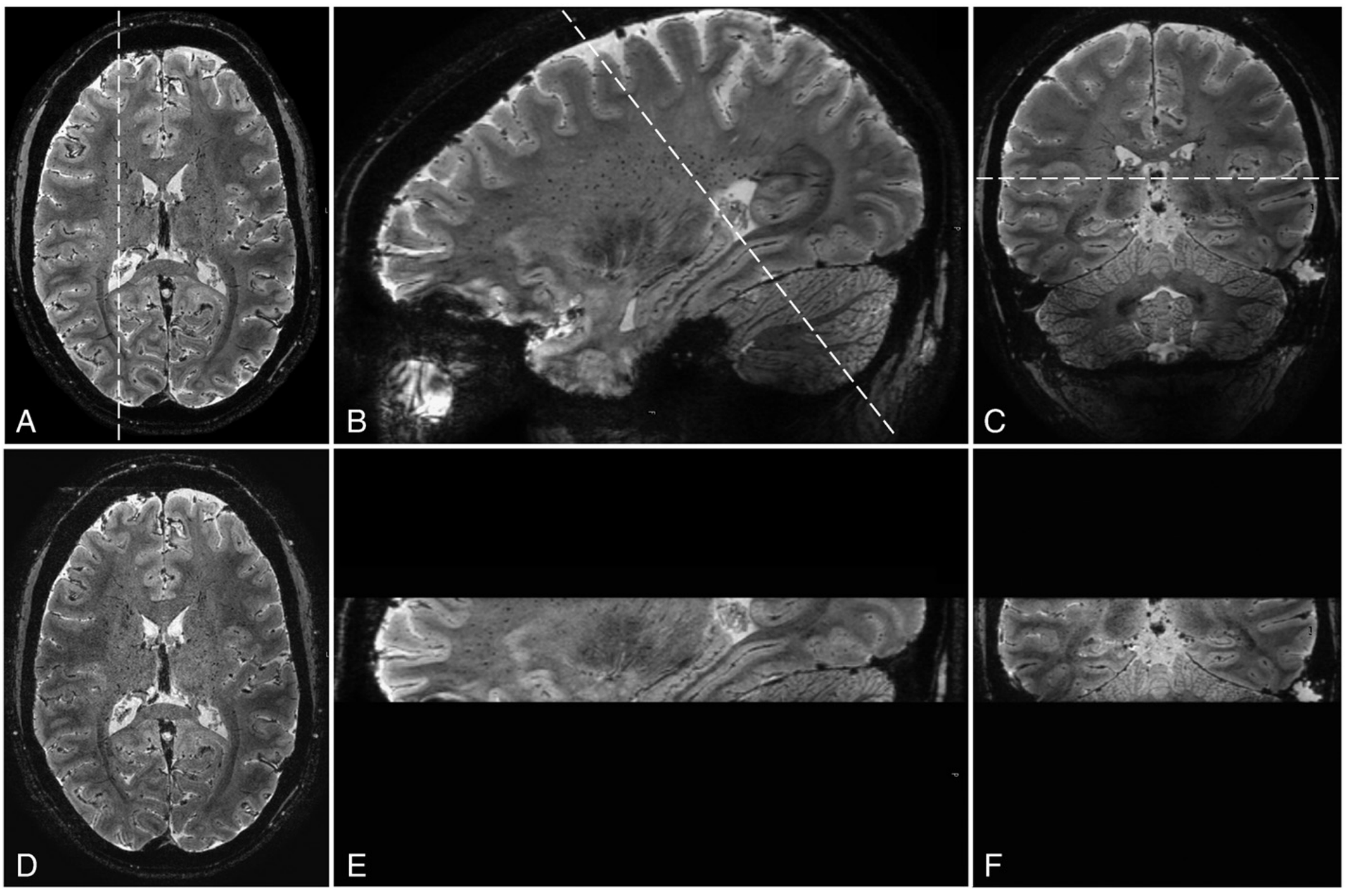

Fig. 1. Magnitude images of the 3D EPI protocol (A: transverse, B: sagittal, C: coronal orientation), showing the gain in coverage and SNR as compared to the 3D GRE imaging protocol (D, E and F). Note that the EPI and GRE images are acquired with the same scan duration and resolution. The dotted lines indicate the perpendicular cross-sections of the different orientations. Some blurring can be seen for the GM just above the nasal cavity in panel B.

Multiplexed EPI

Multiplexed Echo Planar Imaging for Sub-Second Whole Brain FMRI and Fast Diffusion Imaging

David A. Feinberg[1,2,3]*, Steen Moeller[4], Stephen M. Smith[5], Edward Auerbach[4], Sudhir Ramanna[1], Matt F. Glasser[6], Karla L. Miller[5], Kamil Ugurbil[4], Essa Yacoub[4]

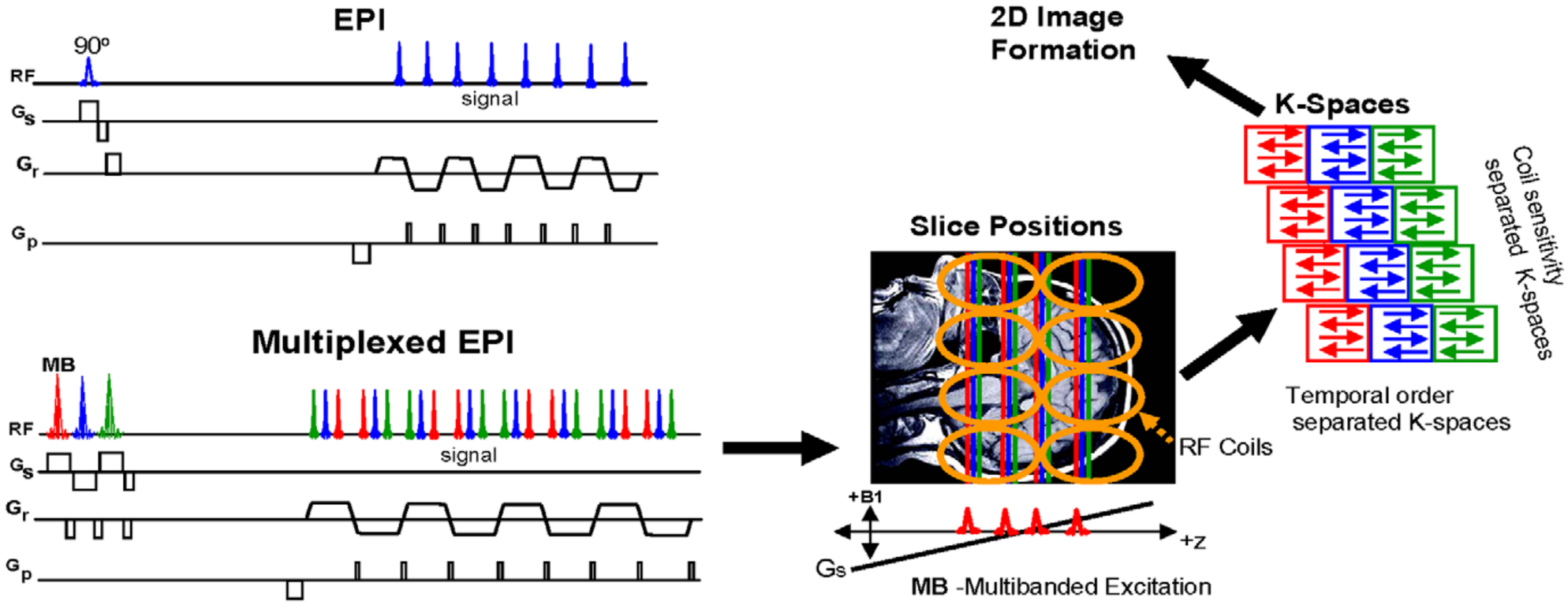

Figure 1. Description of the M-EPI pulse sequence compared with conventional EPI. Top) EPI pulse sequence generates a single image during each readout which is repeated by the number of slices to scan the whole brain. **Bottom**) Multiplexed-EPI (M-EPI) pulse sequence generates several images during a single echo train readout and thus requires fewer repeats to scan the whole brain. The multibanded (MB) RF excitation pulses are the sum of *n* frequency offset sinc-modulated pulses which excite slices at widely spaced positions to improve the separation of signal from the different receiver coils. (Slice Positions) show closely spaced SIR images (red, blue, green) and the excitation positions of the *n* sinc pulses of the first MB pulse. The MB pulse is repeated *m* times for SIR excitations and corresponding signals (red, blue, green) are separated (K-Spaces) into individual k-spaces according to their temporal order in the signal readout period. The MB signals (same color) are further separated into k-spaces using the differential coil sensitivity. 2D FT image reconstruction of each individual k-space data set gives $m \times n$ number of M-EPI images.
doi:10.1371/journal.pone.0015710.g001

Multiplexed EPI

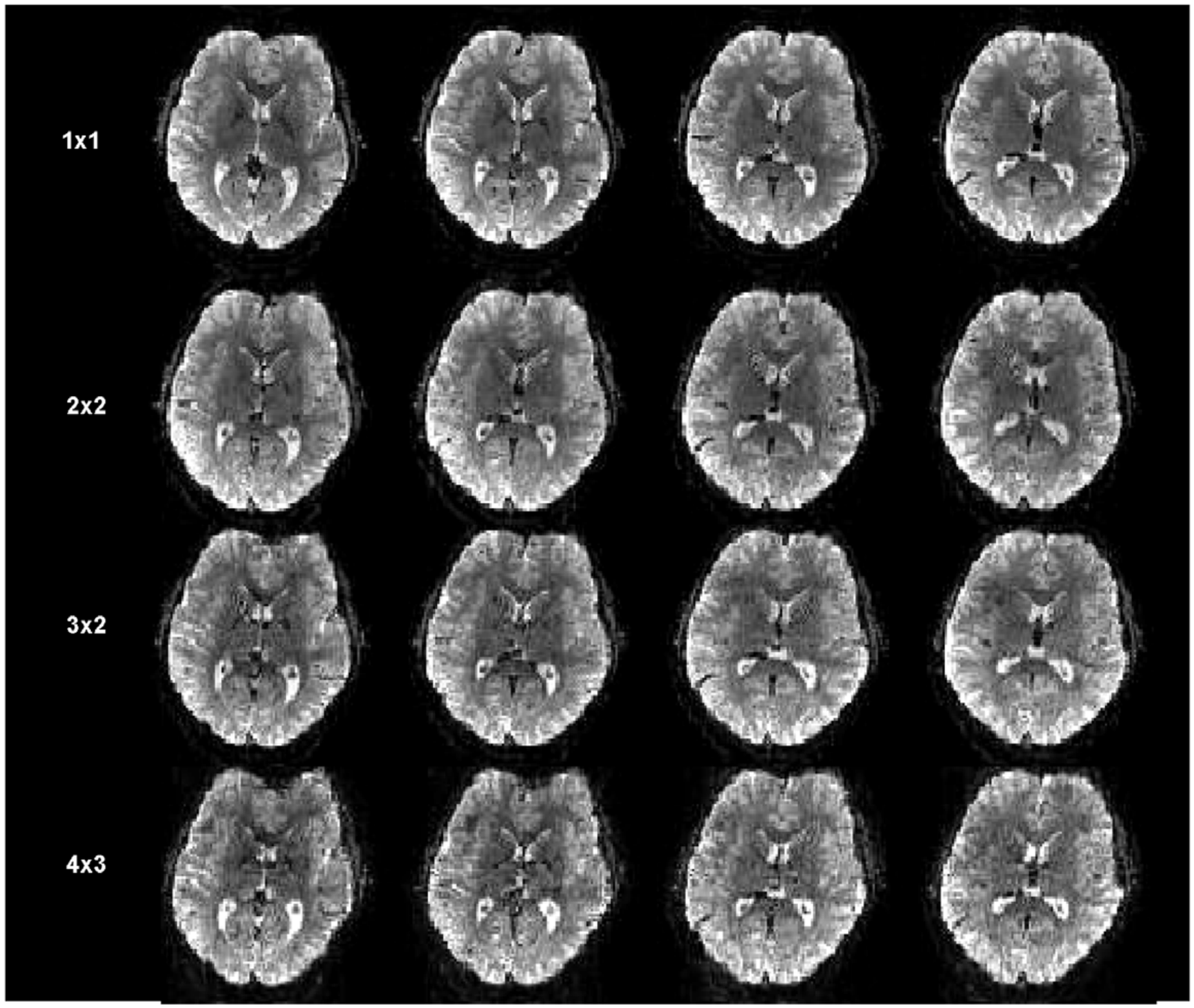

Figure 2. Images at 3 Tesla, comparing 4 adjacent slices out of the total 60 slices at 2mm isotropic resolution covering the entire brain. Each row of images was obtained with a different pulse sequence and slice acceleration, producing 1, 4, 6 and 12 slices from the EPI echo train. The *mxn* parameters (SIR× MB) are shown.
doi:10.1371/journal.pone.0015710.g002

Multiplexed EPI - 7T

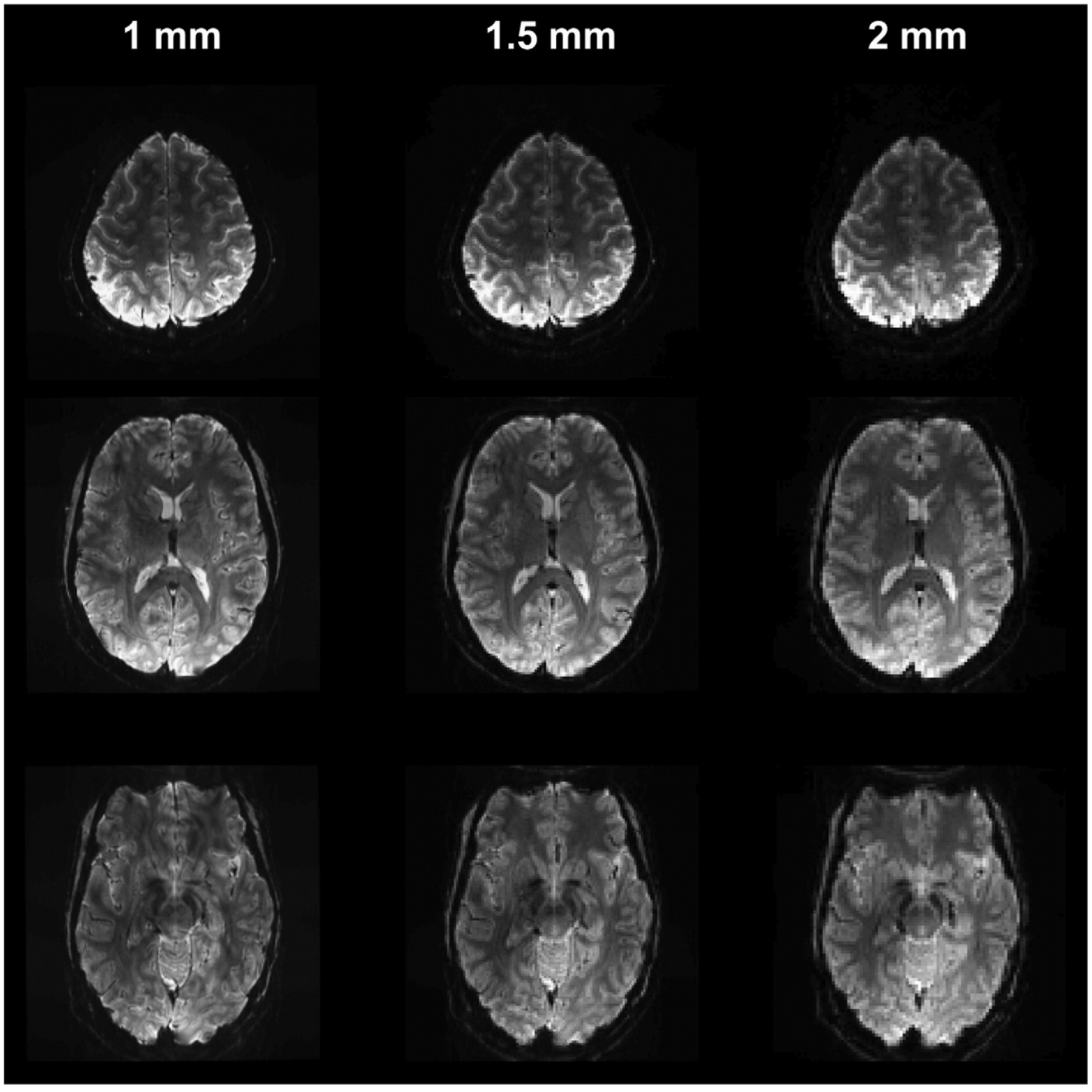

DeMartino et al. NeuroImage 57 2011

Different Contrast

Susceptibility contrast

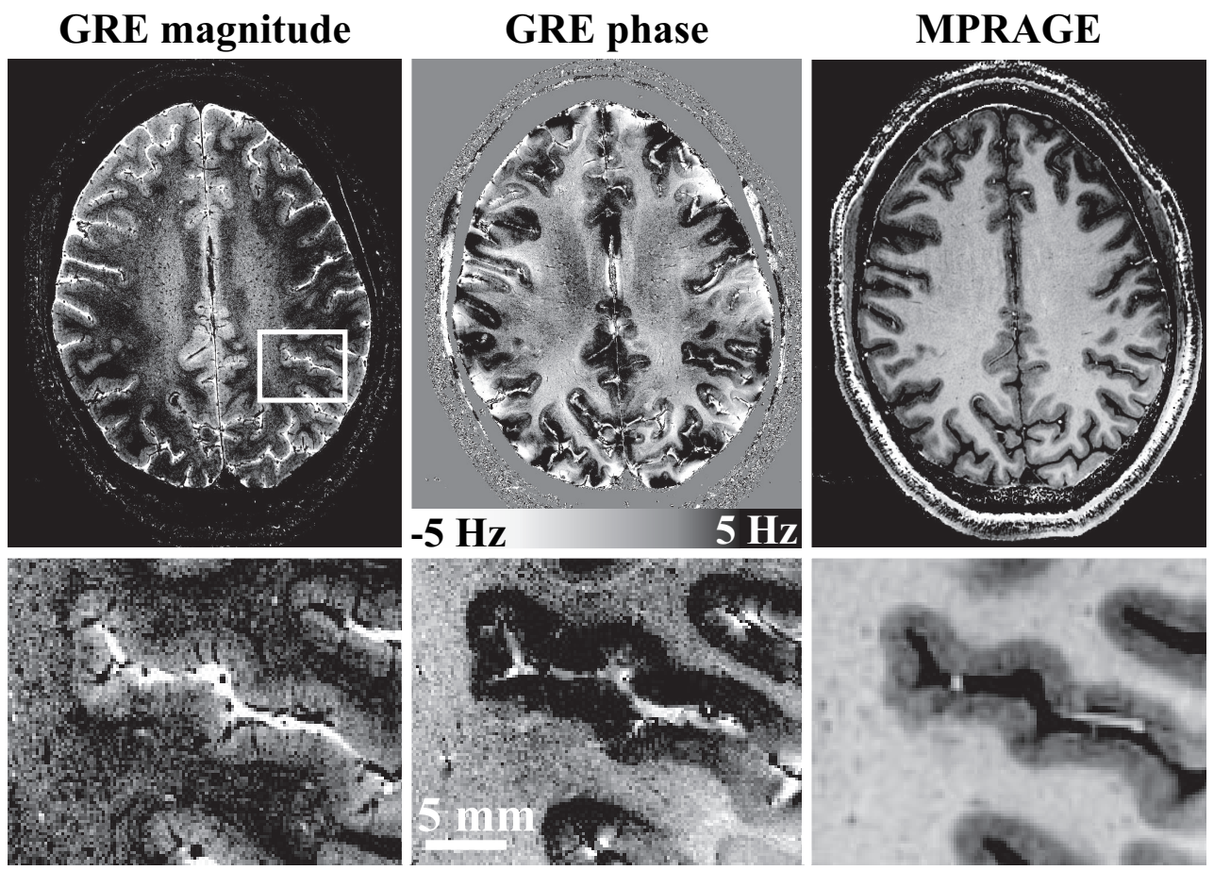

Fig. 1. Illustration of image quality of MRI based on image phase. The increased CNR available with MRI phase data allows dramatically improved resolution and shorter scan time. The GRE data (*Left* and *Center*) were acquired at a resolution of 240 × 240 μm in a scan time of 6.5 min, whereas the MP-RAGE data (*Right*) was acquired at a resolution of 480 × 480 μm in a scan time of 20 min. The scale bar in the GRE phase data shows the frequency shifts corresponding to the observed phase differences. (*Lower*) Magnifications of the area outlined in white on the GRE magnitude image (*Left Upper*). The macroscopic intensity variations in the phase image are attributed to susceptibility effects related to air–tissue interfaces.

High-field MRI of brain cortical substructure based on signal phase

Jeff H. Duyn†, Peter van Gelderen, Tie-Qiang Li, Jacco A. de Zwart, Alan P. Koretsky, and Masaki Fukunaga

11796–11801 | PNAS | July 10, 2007 | vol. 104 | no. 28

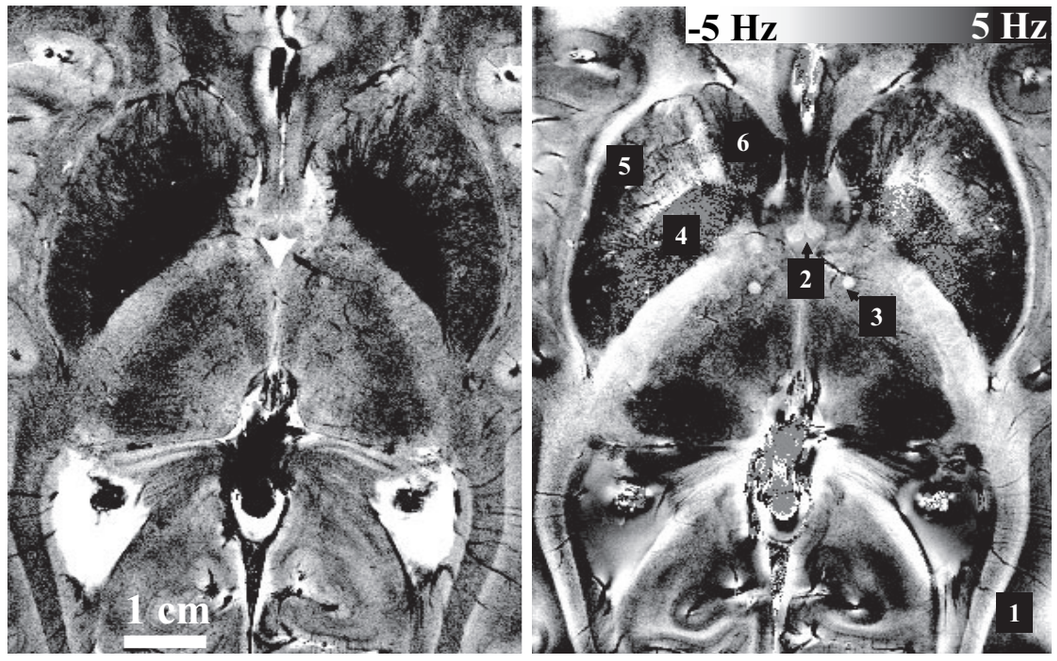

Fig. 2. Example of GRE magnitude and phase data in central brain region acquired at a 240 × 240 μm inplane resolution. Note the many anatomical details visible at this resolution, including veins crossing the optic radiations (box 1), columna fornix (box 2), cross-section of the mamillothalamic tract (box 3), globus pallidus (box 4), putamen (box 5), and head of the caudate nucleus (box 6).

Susceptibility contrast

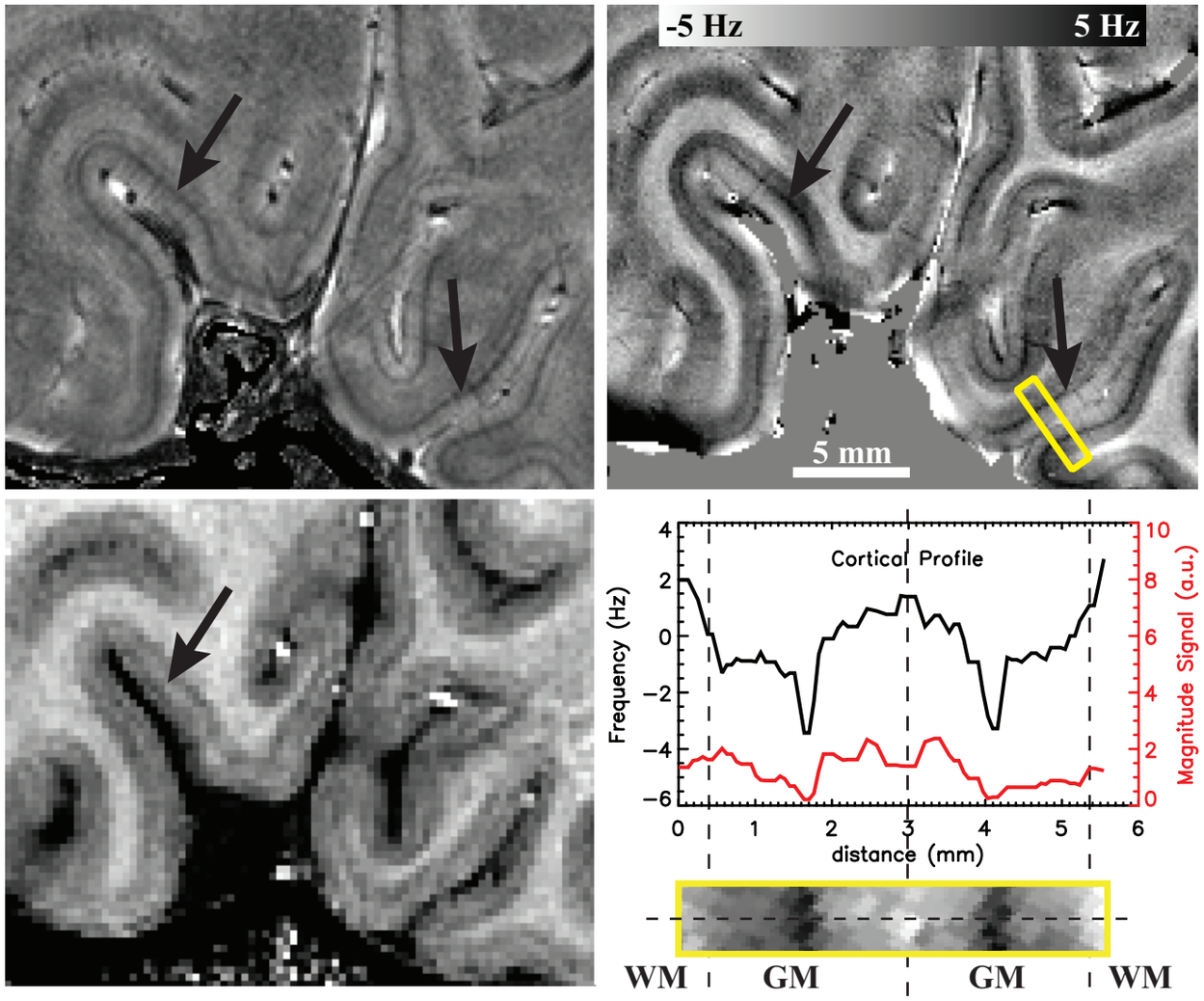

Fig. 4. Intracortical contrast in the primary visual cortex. In the GRE magnitude image (*Left Upper*) and phase image (*Right Upper*), a darkening is observed in the central layers of the cortex, resembling the stria of Gennari (black arrow). Intensity profiles along a single projection through the cortex (dotted line in zoomed area outlined by yellow box) show that this area is ≈150–250 μm wide (*Right Lower*). Note the superior CNR of the phase data compared with the magnitude data (all GRE data are displayed at identical noise levels). The observed frequency difference between central GM and WM reaches ≈6.0 Hz. Regions with central darkening in phase show a faint brightening in the MPRAGE image (*Left Lower*).

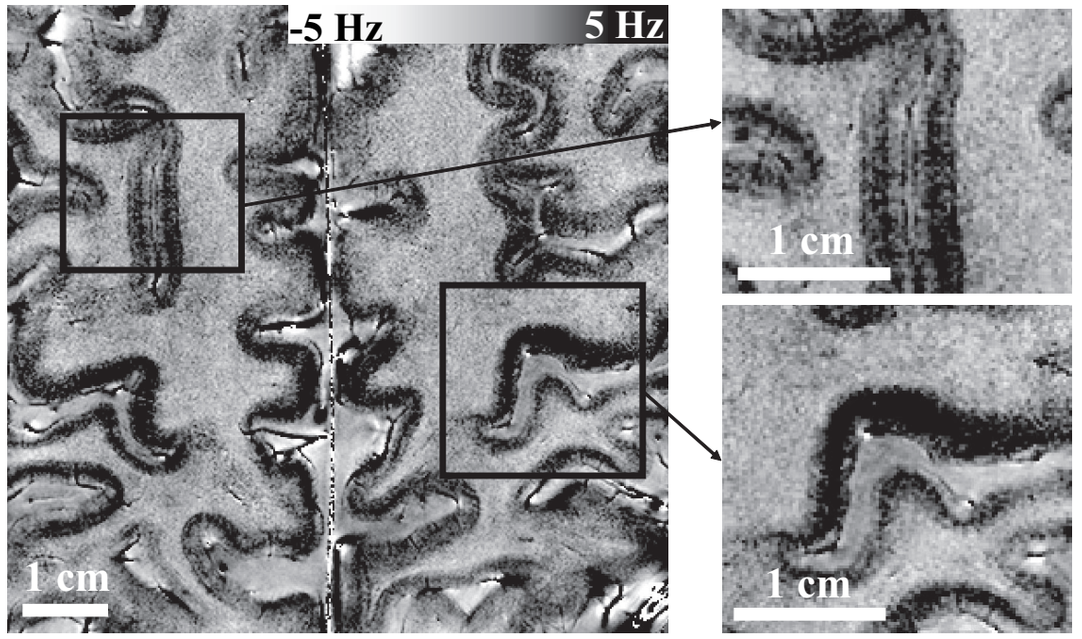

Fig. 3. Intracortical contrast in MRI signal phase. Most cortical regions show a variation intensity that is suggestive of an underlying layer structure (*Left*). The intensity pattern varies between the different gyri, with clear differences between the upper and lower banks of the central sulcus (*Right Lower*) and cortices adjacent to the superior frontal sulcus (*Right Upper*).

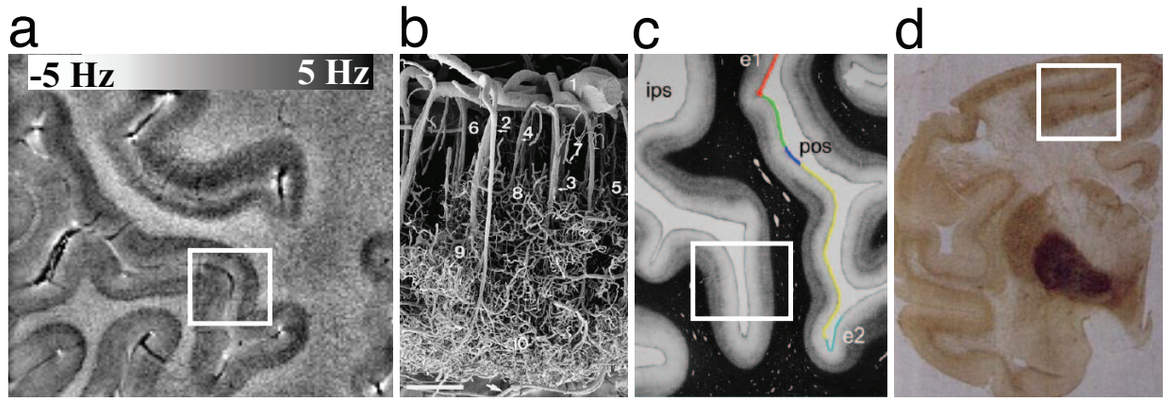

Fig. 5. Illustration of possible origins of MRI phase contrast. (*Insets*) Cortical areas with layer-specific contrast. The increasing contrast seen in the deeper layers of the cortex (*a*, our data) is consistent with multiple hypothesized origins, including vascular density/hemoglobin content (*b*; corrosion cast of cortical vasculature reproduced from ref. 38), myelin concentration (*c*; myelin silver stain reproduced from ref. 39), and iron concentration (*d*; Perl's iron stain reproduced from ref. 44).

Imaging Multiple Sclerosis

Pascal Sati, Maria Gaitan, Danny Reich

7T for Multiple Sclerosis

T1w MPRAGE
0.7 mm^3 iso

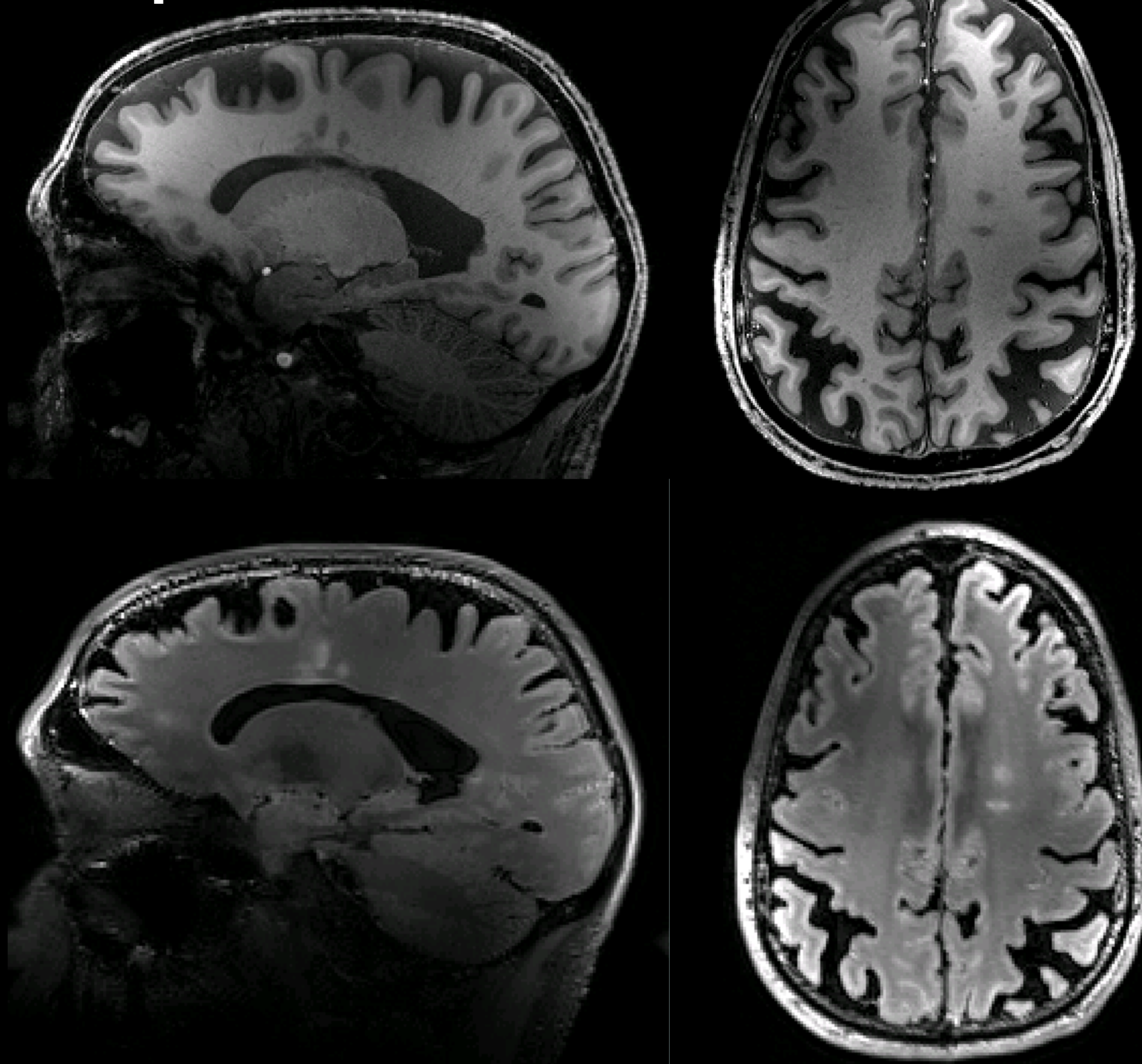

T2w FLAIR
1 mm^3 iso

PS, MG, DR

Post-Gad

T1w MPRAGE
0.7 mm^3 iso

Max Intensity Projection

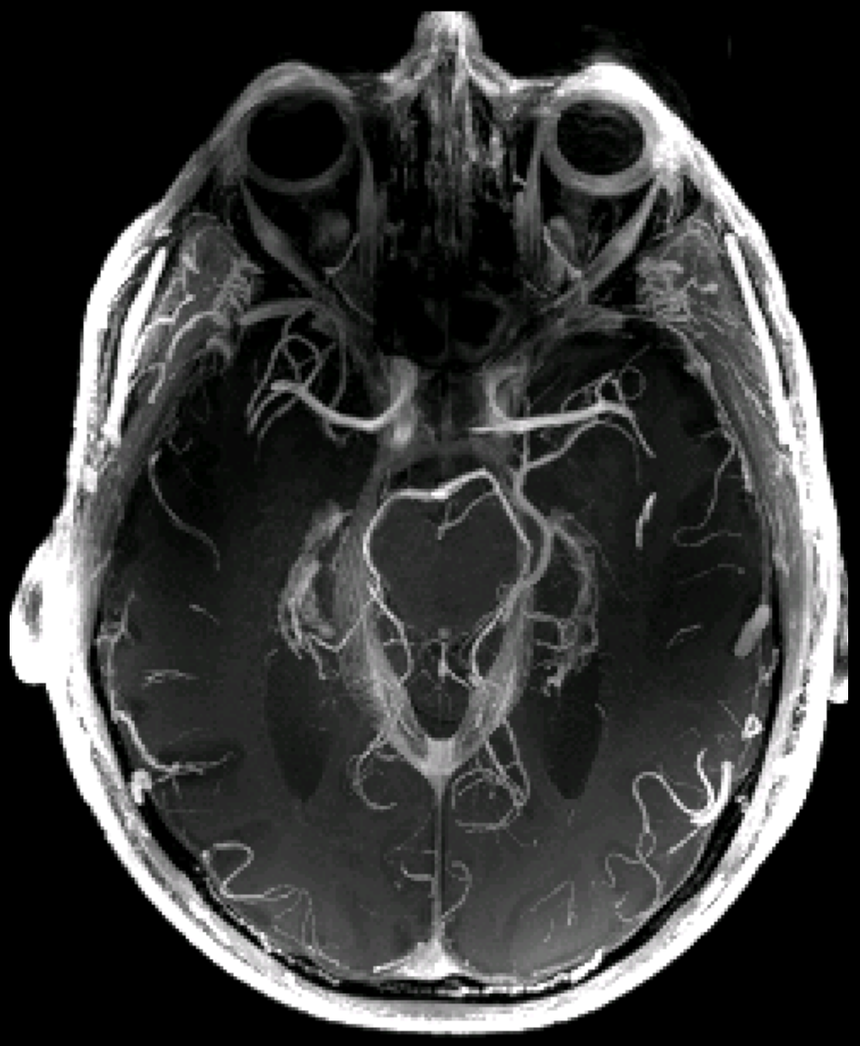

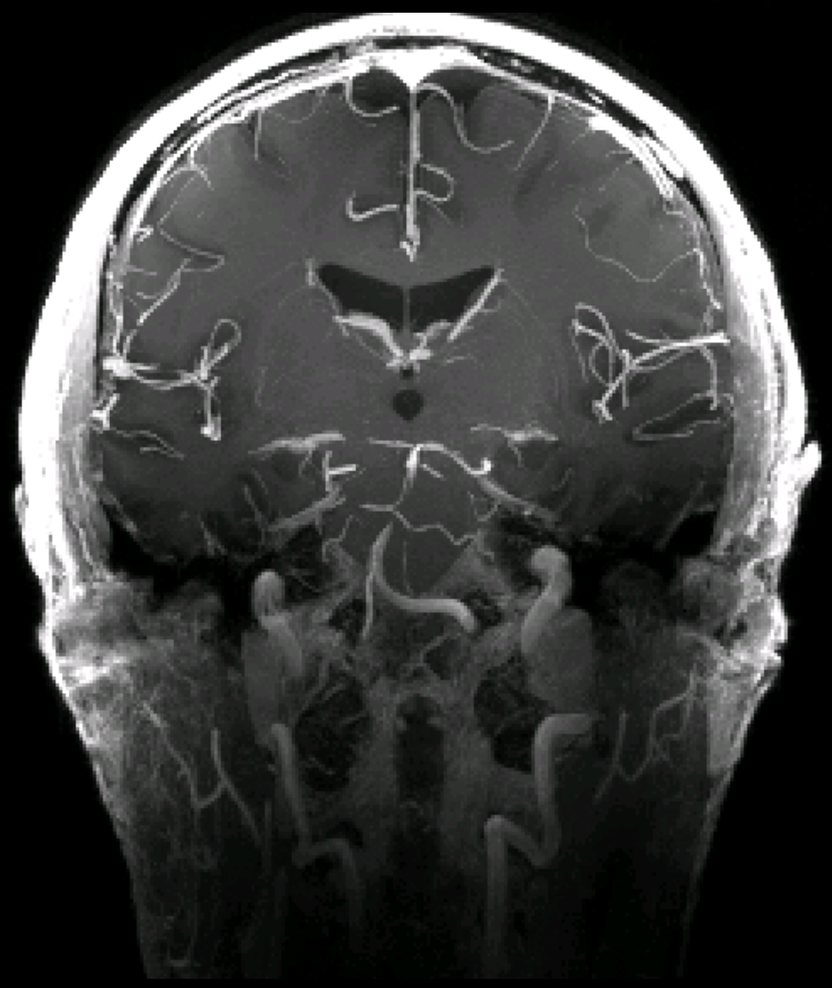

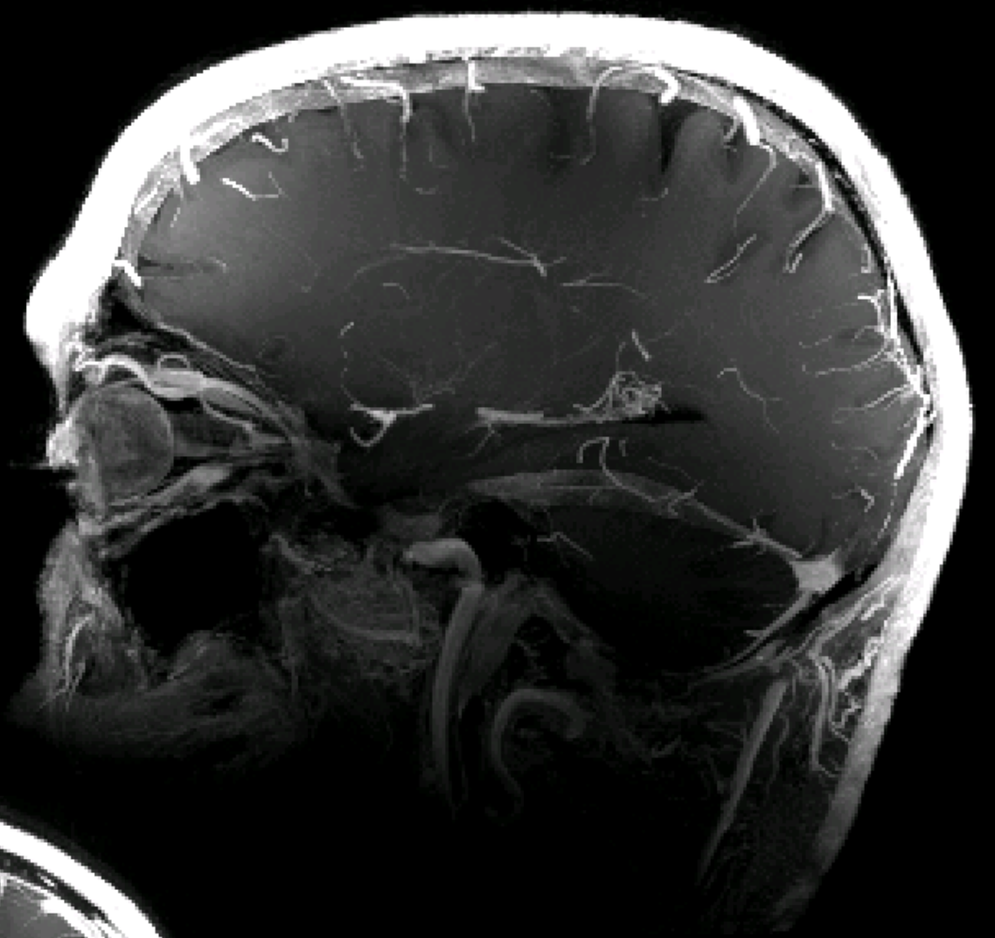

PS, MG, DR

High-resolution GRE imaging in MS

T_2^* weighting (0.25x0.25x1.5 mm^3)

PS, MG, DR

T_2^* and Phase contrast in MS

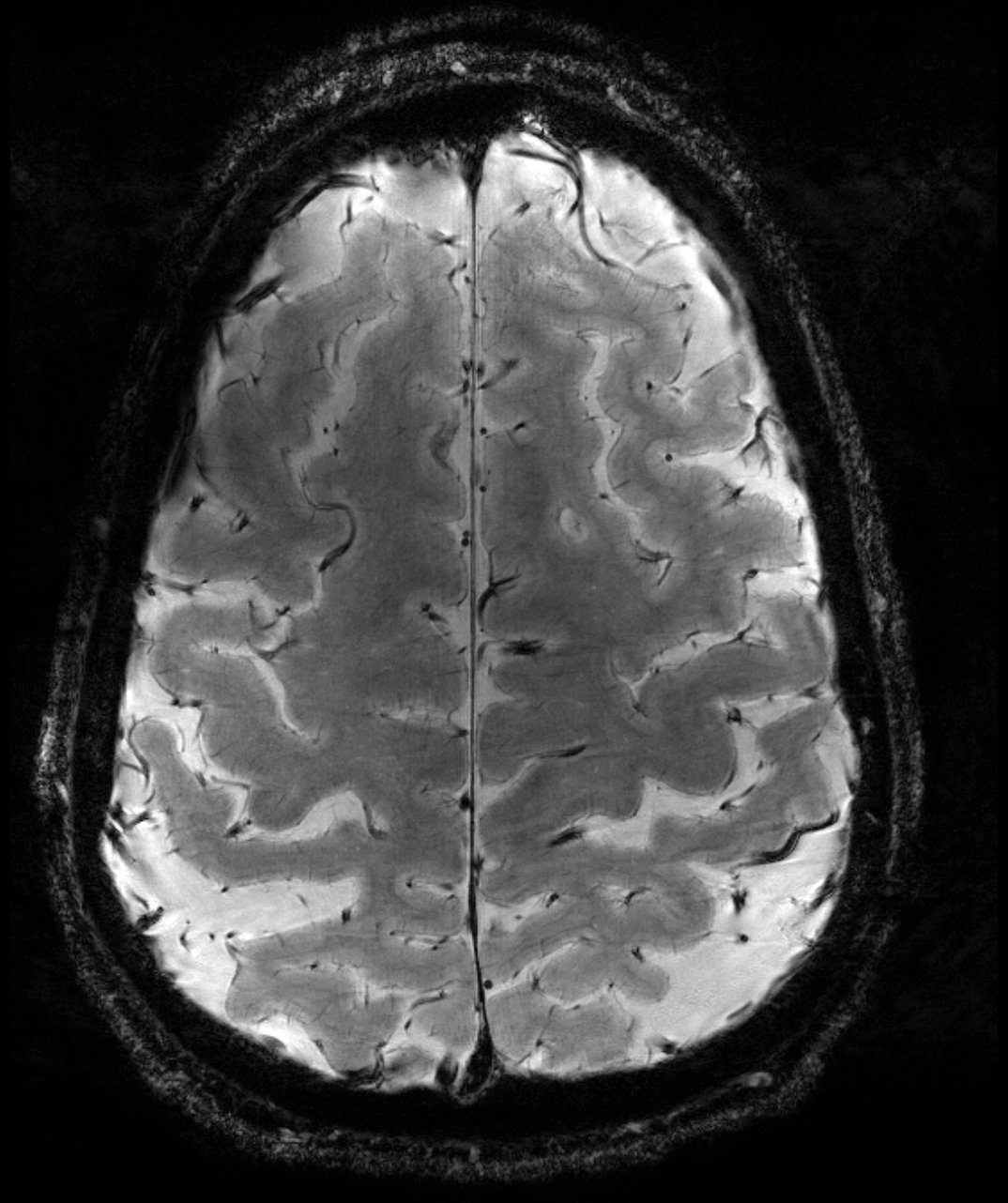

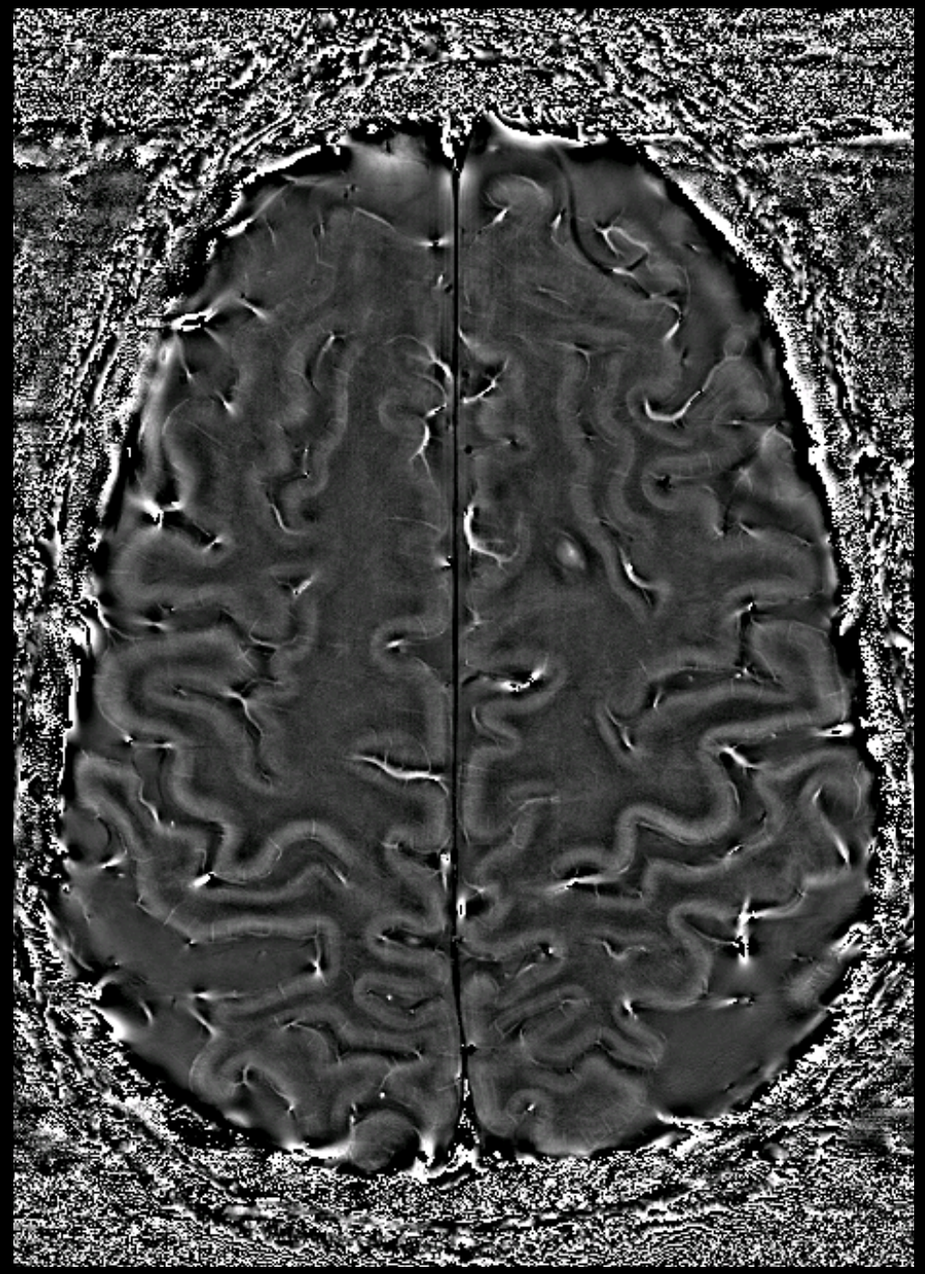

T_2^* weighting (0.25x0.25x1.5 mm^3)

PS, MG, DR

High-resolution GRE imaging in MS

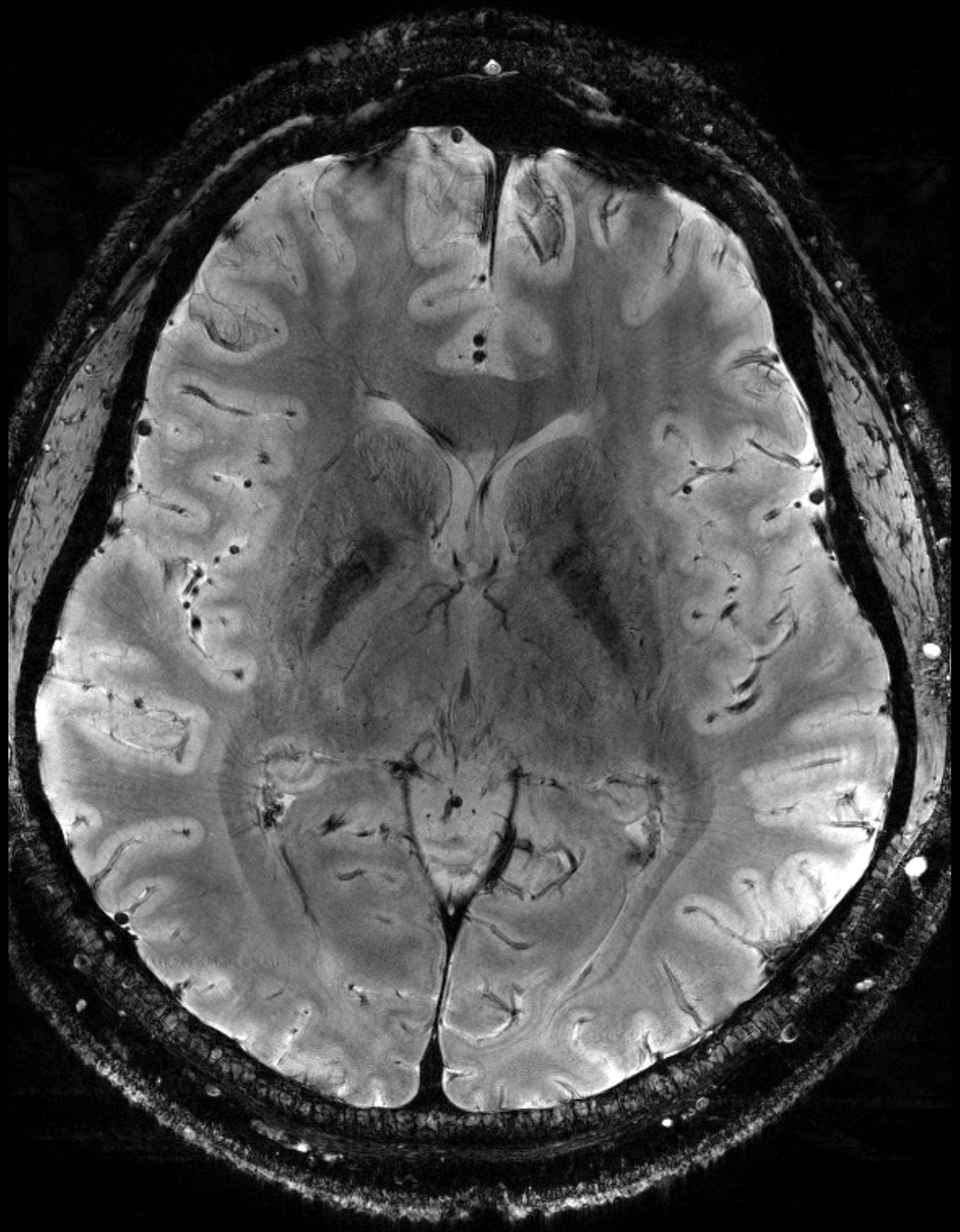

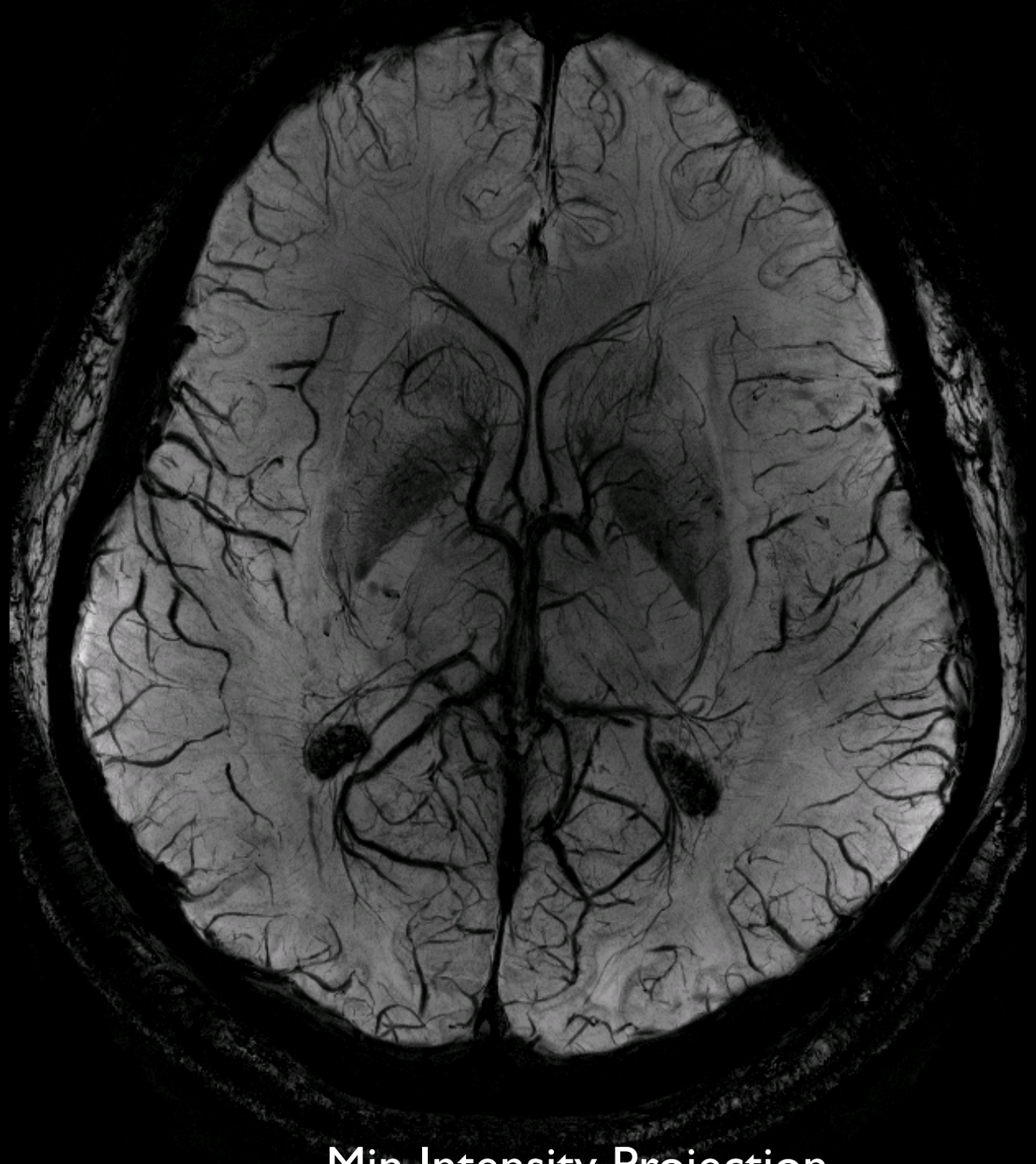

Min Intensity Projection

T_2^* weighting (0.25x0.25x1.5 mm^3)

PS, MG, DR

High-resolution GRE imaging in MS

Min Intensity Projection

T_2^* weighting (0.25x0.25x1.5 mm^3)

PS, MG, DR